PHYSICAL REVIEW B **86**, 035422 (2012)

Weak localization and antilocalization in topological insulator thin films with coherent bulk-surface coupling

Ion Garate and Leonid Glazman
Department of Physics, Yale University, New Haven, Connecticut 06520, USA
(Received 6 June 2012; published 16 July 2012)

We evaluate quantum corrections to conductivity in an electrically gated thin film of a three-dimensional topological insulator. We derive approximate analytical expressions for the low-field magnetoresistance as a function of bulk doping and bulk-surface tunneling rate. Our results reveal parameter regimes for both weak localization and weak antilocalization, and include diffusive Weyl semimetals as a special case.

DOI: 10.1103/PhysRevB.86.035422 PACS number(s): 73.20.Fz, 73.50.−h, 73.25.+i

I. INTRODUCTION AND OVERVIEW

The theoretical discovery[1] of three-dimensional (3D) topological insulators (TIs) in 2006 precipitated an avalanche of experiments aimed at detecting the signature behavior of these unconventional solids. Since then, angle-resolved photoemission spectra[2] have given evidence for the Dirac-type dispersion and the momentum-dependent spin texture of TI surface states, whereas local STM probes have indicated a characteristic suppression of backscattering off surface imperfections.[3] However, the most desired observation of a hallmark dc conduction confined to the surface layer of a 3D TI remains elusive.[4] The main problem is conduction through the bulk: 3D TIs are narrow-gap semiconductors, rich in bulk carriers that are either thermally activated and/or donated by crystalline lattice imperfections. Along with attempts to reduce bulk charge carriers, experimentalists are developing techniques which allow us to register a separate conduction channel on the surface of a 3D TI.[5] Chief among these are measurements of low-field magnetoresistance combined with electrostatic gating of thin-film samples.[6–12]

Low-field magnetoresistance measurements unveil the interference correction $\delta\sigma$ to the Drude conductivity σ_D.[13] At low temperatures, σ_D is defined by independent acts of scattering of electrons off the crystal's imperfections, and is proportional to the classical diffusion constant D. When the phase relaxation length l_ϕ is parametrically longer than the scattering mean-free path, quantum interference affects the conductivity to a measurable extent. The sign of the interference correction depends on the strength of spin-orbit interactions. For weak spin-orbit interactions ($l_{so} \gg l_\phi$, where l_{so} is the spin-orbit scattering length), it follows that $\delta\sigma < 0$. This is called weak localization (WL). In contrast, strong spin-orbit interaction ($l_{so} \ll l_\phi$) leads to suppression of backscattering and thus $\delta\sigma > 0$. This is called weak antilocalization (WAL). Being interference effects, WL and WAL are degraded by a magnetic field H when $H \gtrsim H_\phi \equiv \Phi_0/(8\pi l_\phi^2)$, where $\Phi_0 = h/e$ is the flux quantum. Yet, σ_D is nearly immune to H at such low fields. Therefore, the low-field magnetoconductivity reads as $\Delta\sigma(H) \equiv \sigma(H) - \sigma(0) \simeq \delta\sigma(H) - \delta\sigma(0)$.

All experiments to date report WAL in 3D TI thin films,[14] and ascribe it to the strong spin-orbit interaction in the electronic bands of these materials. For film thickness less than l_ϕ, the measured $\Delta\sigma(H)$ agrees well with the functional form provided by 2D WAL theory, namely,

$$\Delta\sigma(H) \simeq \alpha\,(e^2/2\pi^2\hbar)\,f(H_\phi/H), \tag{1.1}$$

where $f(z) \equiv \ln z - \psi(1/2 + z)$, with ψ and α being the digamma function and a number,[15] respectively. In a system with a single conduction channel, α is universal and equals $1/2$. The WAL contributions add for systems which are isolated from each other. For example, having two independent parallel conduction channels yields $\alpha = 1$, irrespective of the ratio of Drude conductivities of the two subsystems.

The relation between α and the number of parallel channels is at the heart of recent magnetoresistance experiments in 3D TIs.[7,10,11] Overall, the coefficient α is found to depend on the gate voltage. For some devices,[7,10,11] it changes from $\alpha = 1/2$ all the way to $\alpha = 1$. A plausible interpretation for this variation is presented in Ref. 11. At zero or positive bias applied to the top gate, electrons from the n-doped bulk reach the surface states easily: the entire film acts as a single electron system, and $\alpha = 1/2$. At negative bias, electrons are repelled from the top surface and, for strong enough bias, a depletion layer is formed adjacent to it. This depletion region separates the film into two subsystems: bulk carriers (combined with surface carriers from the bottom surface) on one side, and top-surface carriers on the other side. For a wide enough depletion layer, $\alpha = 1$.

In spite of the ongoing scrutiny on the experimental front, quantum corrections to conductivity in 3D TIs have stimulated relatively little theoretical activity. Even though the WAL contribution from TI surface states has been calculated explicitly,[16,17] there are no calculations that incorporate conducting 3D bulk states. The main reason for this omission may be the prevailing view that quantum corrections originating from bulk TI states ought to be conceptually identical to those in ordinary strongly spin-orbit coupled systems, i.e., of WAL type. Recently, an objection to this viewpoint has been raised,[18] declaring that quantum-well states in ultrathin TI films may contribute via WL rather than WAL. Although suggestive, the calculation of Ref. 18 is limited to quasi-two-dimensional (2D) films and disregards the coupling between bulk and surface states, which leaves out several experiments of interest. Besides, its extrapolation to 3D bulk states has not been carried out properly.

In this paper, we evaluate $\Delta\sigma$ for gated 3D thin films as a function of the bulk-carrier concentration and accounting for

the coupling between surface and bulk states. Our calculation applies to TI films that are thicker than the bulk mean-free path, thinner than l_ϕ, and not highly doped. In these films, bulk carriers are three dimensional and are concentrated around the Γ point of the electronic band structure. The resulting approximate analytical expressions for $\Delta\sigma$ [Eqs. (2.35), (3.17), and (3.19)] are aimed at improving the interpretation of magnetoresistance measurements in TIs, in Weyl semimetals,[19] and in some class of topologically trivial materials. Although a few of our observations resemble those developed for graphene[20] and 2D TIs,[17] there are qualitative differences originating from the 3D Dirac nature of bulk carriers in 3D TIs.

Altogether, the results reported here paint a richer picture than previously anticipated. On one hand, we confirm the conventional crossover between $\alpha = 1/2$ and 1 as a function of the gate voltage: the former corresponds to the case of coherently coupled bulk and surface electron states, while the latter indicates a single decoupled Dirac cone on the top surface along with generic WAL from the rest of the film (containing coupled bulk and bottom surface). On the other hand, less conventional results arise when the Fermi energy is close to the bulk band edge or when the Fermi energy is much larger than the bulk band gap: in the former regime, the bulk exhibits WL with $\alpha = -1$, whereas in the latter regime the bulk exhibits an anomalous WAL with $\alpha = 1$. These two "unusual" bulk regimes, combined with the surface contributions, may result in a range of α including $\alpha < 0$ and $\alpha > 1$.

The rest of this work is organized as follows. In Sec. II, we evaluate quantum corrections to *bulk* conductivity. Readers not interested in technical details should read Sec. II A and quickly scan through Secs. II B and II D in order to get acquainted with the nomenclature; the main results of the section are collected in Sec. II D. The well-known message from Sec. II A is that at low energies, bulk electrons of TI films behave as massive 3D Dirac fermions with spin and valley (or orbital) degrees of freedom. The direction of spin is locked with that of momentum, and valleys are coupled to one another by the mass of the Dirac fermions. The special case in which the Dirac mass vanishes is a time- and inversion-symmetric Weyl semimetal.

In Sec. II D, we identify and count the number of "soft" cooperon modes, which determine the magnitude and sign of $\Delta\sigma$ in the bulk. Each soft cooperon obeys a classical diffusion equation and is thus associated with a conserved physical quantity. Since charge is conserved, there is at least one soft cooperon in (nonmagnetic) bulk TIs. We find that additional soft cooperons can emerge depending on the bulk doping concentration as well as the bulk band gap. This realization leads to the most important results in Sec. II D [Eqs. (2.33)–(2.35)], which indicate that for bulk states α may acquire three different universal values. On one hand, WL with $\alpha = -1$ is possible when the bulk Fermi surface is "small" (as defined in the text) because in this case the spin-momentum locking of bulk states becomes weak and the spin of electrons is nearly conserved. In contrast, WAL with $\alpha = 1$ can arise for bulk TIs with particularly small band gaps because in such case bulk electrons can be described by a 3D analog of graphene with two nearly decoupled valleys, each contributing $1/2$ to α. For a more generic case, in which neither valley nor spin are approximately conserved, the quantum interference is similar to that of an ordinary film with strong spin-orbit coupling and therefore $\alpha = 1/2$. Magnetic fields perpendicular to the TI film can be used to induce crossovers between different universal regimes of α. The accessible values of α and the corresponding crossover fields depend on the bulk electron density.

In Sec. III, we evaluate the *full* $\Delta\sigma$ in 3D TI thin films, which comprises coupled bulk and surface contributions. Sections III A and III B cover preliminary material that is needed to derive the main results in Sec. III C. Section III A reviews the well-established fact that, in absence of magnetic order, isolated TI surface states exhibit WAL with $\alpha = 1/2$ (in this paper we assume one Dirac cone per surface). Section III B develops a diagrammatic framework for evaluating quantum corrections to conductivity in ordinary tunnel-coupled layers. Readers who are not interested in technicalities can disregard the diagrams in the figures and concentrate on the outcome of the calculation [Eqs. (3.8)–(3.12)], as well as on the subsequent discussion. One qualitative point made therein is that the crossover from weak to strong coupling (which is accompanied by a change in α from 1 to $1/2$) occurs when the interlayer resistance for a square of area l_ϕ^2 becomes smaller than the sum of the classical intralayer resistances.

Section III C combines results from Secs. II D, III A and III B in order to figure out quantum corrections to conductivity in experimentally realized thin films. The most important results in Sec. III C are Eqs. (3.17) and (3.19), which describe how $\Delta\sigma$ depends on the bulk doping concentration, on the phase relaxation rate, and on the bulk-surface tunneling rate. Some special cases of these results are highlighted in Appendix F. A salient conclusion is that the WL regime of isolated bulk states is generally eliminated when either one of the film surfaces is strongly coupled to bulk states, in which case the film displays $1/2 \leqslant \alpha \leqslant 1$. However, WL can still be present if the TI surfaces have short phase relaxation lengths.

Finally, Sec. III D characterizes the electrostatics of the depletion layer and estimates the bulk-surface tunneling rate in TI films. This estimate confirms experimental indications showing that both weak and strong bulk-surface coupling are accessible by mediation of a gate voltage.

II. QUANTUM CORRECTIONS TO BULK CONDUCTIVITY

This section is devoted to evaluating $\delta\sigma$ for the bulk states of a 3D TI. As a by-product, we derive $\delta\sigma$ for a time-reversal symmetric Weyl semimetal. The contribution from TI surface states will be discarded until the next section.

A. Model

The bulk band structure of a 3D TI near the Γ point can be approximated by the following $\mathbf{k}\cdot\mathbf{p}$ Hamiltonian:[21]

$$\mathcal{H} = \sum_{\mathbf{k}} \Psi_{\mathbf{k}}^\dagger h(\mathbf{k}) \Psi_{\mathbf{k}},$$
$$h(\mathbf{k}) \simeq \epsilon(\mathbf{k})\mathbf{1}_4 + M(\mathbf{k})\mathbf{1}_2\,\tau^z + \hbar(v_z k_z \sigma^z + v_\perp \mathbf{k}_\perp\cdot\boldsymbol{\sigma}^\perp)\tau^x, \tag{2.1}$$

where $\boldsymbol{\tau}$ is an orbital pseudospin ($\tau^z = T, B$), $\boldsymbol{\sigma}$ is the real spin ($\sigma^z = \uparrow,\downarrow$), $\mathbf{k} = (\mathbf{k}_\perp, k_z)$ is the momentum measured from the Γ point of the Brillouin zone, $\mathbf{1}_N$ is an $N\times N$

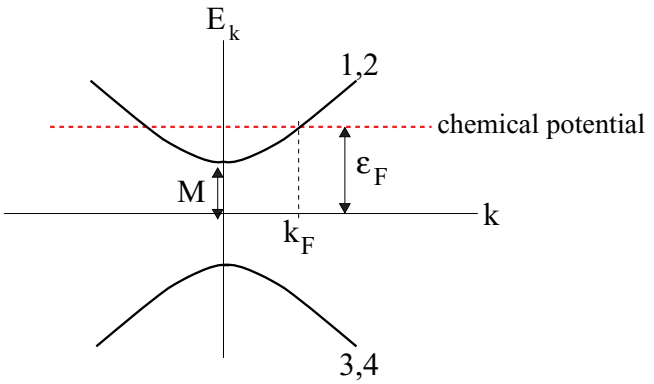

FIG. 1. (Color online) Bulk energy bands of an n-doped 3D TI near the Γ point, in the spherical approximation. The momentum k is measured from the Γ point. The energies ϵ_F and M are measured with respect to midgap.

identity matrix, $\Psi = (\Psi_{T\uparrow}, \Psi_{T\downarrow}, \Psi_{B\uparrow}, \Psi_{B\downarrow})$ is a four-spinor, $\epsilon(\mathbf{k}) = \epsilon(-\mathbf{k})$ is the part of the Hamiltonian that is independent of spin/pseudospin indices, v_z and $v_\perp$ are the Fermi velocities, and $M(\mathbf{k}) = M_0 - M_1 k_\perp^2 - M_2 k_z^2$ is the mass term (independent of spin). M_0, M_1, and M_2 are constants.

Equation (2.1) captures the bottom of the conduction band and the top of the valence band in the vicinity of the Γ point ($k \equiv 0$), where the band gap is smallest. It models 3D Dirac fermions with a Dirac mass that equals half the energy gap. For the purposes of this paper, we ignore $\epsilon(\mathbf{k})$, and assume $M(\mathbf{k}) = M = \text{const} > 0$ as well as spherical symmetry ($v_z = v_\perp = v$). These assumptions simplify calculations without incurring a qualitative loss of generality. For instance, the XXZ anisotropy can be modeled by promoting the diffusion constant from a scalar to a matrix. Also, the k^2 terms in $M(\mathbf{k})$ can be incorporated into our final results by $M \to |M(\mathbf{k}_F)|$, where $\mathbf{k}_F$ is the Fermi wave vector. Note that in the absence of spherical symmetry, the Fermi surface does not have a constant mass; this complication will be disregarded in this paper. Finally, $\epsilon(\mathbf{k})$ can be absorbed into the definition of the Fermi energy.

The energy eigenvalues for $h(\mathbf{k})$ in the spherical approximation are $E_{\mathbf{k}\pm} = \pm\sqrt{\hbar^2 v^2 k^2 + M^2}$, each doubly degenerate (Fig. 1). The corresponding Bloch states can be written as

$$|\Psi_{\mathbf{k}\alpha}\rangle = (1/\sqrt{V}) \exp(i\mathbf{k}\cdot\mathbf{r})|\alpha\mathbf{k}\rangle, \tag{2.2}$$

where V is the volume of the TI and $\alpha \in \{1,2,3,4\}$ is a band index (1 and 2 denote conduction bands, while 3 and 4 denote valence bands). This α is obviously unrelated to that of Eq. (1.1); from here on, it will be clear from the context which one we are referring to. For concreteness, we set the chemical potential in the bulk conduction band, although all results obtained in the following will be directly applicable to p-doped bulk TIs as well. The density of conduction band electrons is then

$$n \simeq \frac{\left(\epsilon_F^2 - M^2\right)^{3/2}}{\pi^2 \hbar^3 v^3}, \tag{2.3}$$

where ϵ_F is the Fermi energy measured from the middle of the bulk energy gap. Adopting the basis $\{|T\uparrow\rangle, |T\downarrow\rangle, |B\uparrow\rangle, |B\downarrow\rangle\}$, the two eigenspinors corresponding to the conduction bands near the Γ point are

$$|1\mathbf{k}\rangle = \sqrt{\frac{E_k + M}{2E_k}} \left(1, 0, \frac{\hbar v k_z}{E_k + M}, \frac{\hbar v k_+}{E_k + M}\right),$$
$$|2\mathbf{k}\rangle = \sqrt{\frac{E_k + M}{2E_k}} \left(0, 1, \frac{\hbar v k_-}{E_k + M}, \frac{-\hbar v k_z}{E_k + M}\right), \tag{2.4}$$

where $k_\pm = k_x \pm i k_y$ and $E_k = E_{\mathbf{k},+}$. Since all non-Hall dc transport properties of good conductors involve states close to the Fermi energy, we hereafter ignore valence bands.

Unlike in the $\mathbf{k}\cdot\mathbf{p}$ Hamiltonians for graphene and 2D (or quasi-2D) TIs, Eq. (2.1) can not be decomposed into two 2×2 block-diagonal matrices (due to $M \neq 0$). In addition, the k_z band dispersion absent in 2D can not be neglected in our case. These two features make the calculations and results of this section quite different from those of Refs. 17, 18, and 20.

Equation (2.1) becomes inaccurate when the chemical potential moves up in the conduction band and electron pockets away from the Γ point begin to be populated. These additional pockets contribute to quantum interference, and the total $\delta\sigma$ depends on the scattering rate between different electron pockets. Although a realistic study of the full band structure is beyond the scope of this paper, we expect calculations based on Eq. (2.1) to provide a generic understanding of quantum corrections to conductivity in 3D Dirac materials at low-to-moderate doping concentrations.

B. Formalism

In order to quantify the conductivity of a bulk TI, we begin by characterizing the simplest possible disorder potential: $V_{\text{dis}}(\mathbf{r}) = V(\mathbf{r})\mathbf{1}_4$, which is time independent (elastic) and independent of spin as well as orbital degrees of freedom. For simplicity, we assume $V(\mathbf{r})$ to be slowly varying at the atomic scale, yet short ranged compared to the mean-free path: $V(\mathbf{r}) = V_0\delta(\mathbf{r})$. It is due to its slow spatial variation on atomic length scales that V_{dis} becomes an identity operator in orbital space. With such disorder realization, the Fermi-surface lifetime τ_0 for the $\alpha = 1,2$ eigenstates in Eq. (2.2) obeys

$$\frac{1}{\tau_0} = \frac{2\pi u_0}{\hbar} \int_{\mathbf{k}'} \sum_{\alpha'} |\langle \alpha\mathbf{k}_F | \alpha'\mathbf{k}'_F\rangle|^2 \delta(\epsilon_F - E_{\mathbf{k}'\alpha'})$$
$$\simeq \frac{\pi u_0 \nu}{\hbar}\left(1 + \frac{M^2}{\epsilon_F^2}\right), \tag{2.5}$$

where $\int_{\mathbf{k}} \equiv \int d^3k/(2\pi)^3$, $u_0 \equiv n_i V_0^2$, n_i is the density of impurities, and ν is the density of states per band and per unit volume at ϵ_F.

A related quantity is the transport scattering rate τ^{-1}:

$$\frac{1}{\tau} \equiv \frac{2\pi u_0}{\hbar} \int_{\mathbf{k}'} \sum_{\alpha'} (1 - \hat{\mathbf{k}}_F \cdot \hat{\mathbf{k}}'_F) |\langle \alpha\mathbf{k}_F | \alpha'\mathbf{k}'_F\rangle|^2 \delta(\epsilon_F - E_{\mathbf{k}'\alpha'})$$
$$= \frac{2}{3\tau_0} \frac{\epsilon_F^2 + 2M^2}{\epsilon_F^2 + M^2}. \tag{2.6}$$

The momentum dependence of $|\alpha\mathbf{k}\rangle$ makes $\tau_0 \neq \tau$ even for δ-function impurity potentials. Throughout this work, we impose $(\epsilon_F - M)\tau \gg \hbar$ or equivalently $k_F l \gg 1$, where $l = (D\tau)^{1/2}$

is the elastic mean-free path,

$$k_F = \left(\epsilon_F^2 - M^2\right)^{1/2}/(\hbar v) \tag{2.7}$$

is the Fermi wave vector, and

$$D = v_F^2\tau/3 = v^2\tau\left(1 - M^2/\epsilon_F^2\right)/3 \tag{2.8}$$

is the classical diffusion constant.

Next, we consider a TI with spatial dimensions $L \times L$ in the xy plane and a thickness W along the z direction. We take a thin-film geometry with $L \gg l_\phi \gg l$ and $l_\phi \gg W \gg l$, where $l_\phi = (D\tau_\phi)^{1/2}$ is the coherence length and τ_ϕ is the phase relaxation time. The conductivity of this film is

$$\sigma = \sigma_D + \delta\sigma, \tag{2.9}$$

where σ_D is the classical (Drude) part and $\delta\sigma$ is the part coming from quantum interference.

On one hand, the Drude conductivity can be approximated as

$$\sigma_D \simeq \frac{e^2\hbar}{2\pi}\sum_{\alpha,\beta}\int_{\mathbf{k}} v^x_{\alpha\beta}(\mathbf{k})\tilde{v}^x_{\beta\alpha}(\mathbf{k})G^R_\alpha(\mathbf{k})G^A_\beta(\mathbf{k}), \tag{2.10}$$

where we have assumed a spatially uniform dc electric field and $\alpha,\beta \in \{1,2\}$. $v^x_{\alpha\beta} = \langle\alpha\mathbf{k}|\mathbf{v}\cdot\hat{x}|\beta\mathbf{k}\rangle$ is a matrix element for the x component of the bare velocity operator $\mathbf{v} = v\tau^x\boldsymbol{\sigma}$, which obeys

$$\mathbf{v}_{\alpha\beta}(\mathbf{k}) = \hbar v^2(\mathbf{k}/E_k)\delta_{\alpha\beta} \quad (\text{for } \alpha,\beta \in \{1,2\}). \tag{2.11}$$

Disorder vertex corrections renormalize Eq. (2.11) to

$$\tilde{\mathbf{v}}_{\alpha\beta} = \mathbf{v}_{\alpha\beta}(\tau/\tau_0) \tag{2.12}$$

(see Appendix A). In addition,

$$G^{R(A)}_\alpha(\mathbf{k}) = \left[\epsilon_F - E_{\mathbf{k}\alpha} + (-)\frac{i\hbar}{2\tau_0}\right]^{-1} \tag{2.13}$$

is the zero-frequency retarded (advanced) Green's function in the band eigenstate basis. Using $G^{R(A)}_1(\mathbf{k}) = G^{R(A)}_2(\mathbf{k}) \equiv G^{R(A)}(\mathbf{k})$, Eq. (2.10) yields

$$\sigma_D = 2e^2\nu D. \tag{2.14}$$

On the other hand, the quantum correction $\delta\sigma$ can be written as $\delta\sigma \simeq \delta\sigma_1 + \delta\sigma_2$, represented pictorially in Fig. 2. Following standard approximations, the expression for $\delta\sigma_1$ is

$$\delta\sigma_1 \simeq \frac{e^2\hbar}{2\pi}\sum_{\alpha,\alpha',\beta,\beta'}\int_{\mathbf{k}} \tilde{v}^x_{\alpha\beta}(\mathbf{k})\tilde{v}^x_{\beta'\alpha'}(-\mathbf{k})G^R_\alpha(\mathbf{k})G^R_{\alpha'}(-\mathbf{k}) \times G^A_\beta(\mathbf{k})G^A_{\beta'}(-\mathbf{k})\frac{1}{W}\int\frac{d^2Q}{(2\pi)^2}C^{\beta\beta'}_{\alpha'\alpha}(\mathbf{k},\mathbf{k},\mathbf{Q}). \tag{2.15}$$

In the second line of Eq. (2.13), we have exploited the condition $W \ll l_\phi$, which allows us to set $Q_z = 0$ everywhere. $C^{\beta\beta'}_{\alpha'\alpha}(\mathbf{k}_1,\mathbf{k}_2,\mathbf{Q})$ are the matrix elements of the cooperon matrix $\hat{C}$ in the band eigenstate basis. $\mathbf{Q} = (Q_x, Q_y)$ is the momentum of the cooperon, the magnitude of which ranges from 0 to $\simeq (D\tau)^{-1/2}$. $\hat{C}$ obeys the Bethe-Salpeter equation [Fig. 2(b)]

$$C^{\beta\beta'}_{\alpha'\alpha}(\mathbf{k}_1,\mathbf{k}_2,\mathbf{Q}) = \Gamma^{\beta\beta'}_{\alpha'\alpha}(\mathbf{k}_1,\mathbf{k}_2,\mathbf{Q}) + \int_{\mathbf{k}_3}\Gamma^{\beta\beta''}_{\alpha'\alpha''}(\mathbf{k}_1,\mathbf{k}_3,\mathbf{Q}) \times G^A_{\beta''}(\mathbf{k}_3)G^R_{\alpha''}(-\mathbf{k}_3+\mathbf{Q})C^{\beta''\beta'}_{\alpha''\alpha}(\mathbf{k}_3,\mathbf{k}_2,\mathbf{Q}), \tag{2.16}$$

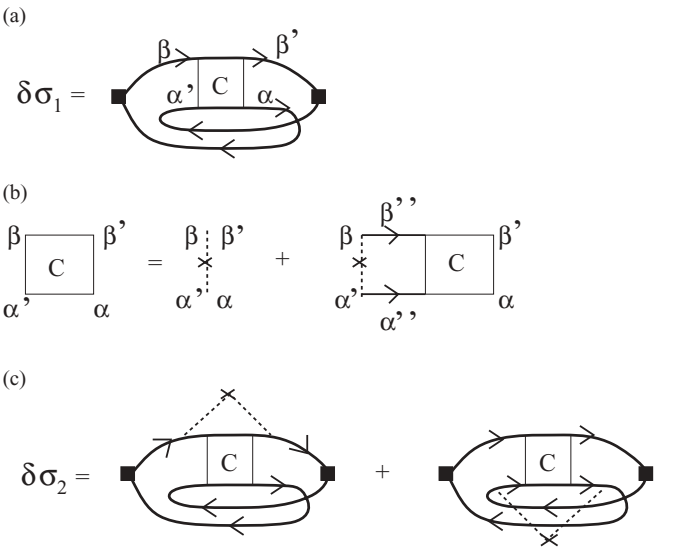

FIG. 2. (a) Feynman diagram for $\delta\sigma_1$, defined in the text. Filled squares denote velocity operators (including disorder vertex corrections), C is the cooperon. (b) Diagrammatic representation of the Bethe-Salpeter equation for the cooperon. Crosses correspond to impurity scattering centers. Solid lines with arrows are disorder-averaged Green's functions. (c) Additional Feynman diagrams that contribute to conductivity of 3D TIs even when impurity scattering is isotropic.

where a sum over repeated indices is implied and

$$\Gamma^{\beta\beta'}_{\alpha'\alpha}(\mathbf{k}_1,\mathbf{k}_2,\mathbf{Q}) \equiv u_0\langle\beta\mathbf{k}_1|\beta' - \mathbf{k}_2 + \mathbf{Q}\rangle\langle\alpha' - \mathbf{k}_1 + \mathbf{Q}|\alpha\mathbf{k}_2\rangle$$

is the bare disorder vertex [first term on the right-hand side of Fig. 2(b)].

Equation (2.16) is a complicated integral equation because $C^{\beta\beta'}_{\alpha'\alpha}$ is a function of three momenta. This is unlike in simplest examples, where the cooperon depends only on $\mathbf{Q}$. The difficulty originates from the momentum dependence of $|\alpha\mathbf{k}\rangle$, which can not be overlooked as it crucially determines both the magnitude and the sign of $\delta\sigma$. One procedure[22] to solve Eq. (2.16) starts by writing the cooperon in the two-particle spin/orbit basis $\{|m,m'\rangle\}$, where $m \in \{T\uparrow, T\downarrow, B\uparrow, B\downarrow\}$:

$$C^{\beta\beta'}_{\alpha'\alpha}(\mathbf{k}_1,\mathbf{k}_2,\mathbf{Q}) = \sum_{m,m',n,n'}\langle\alpha',-\mathbf{k}_1+\mathbf{Q}|m'\rangle\langle\beta\mathbf{k}_1|m\rangle \times\langle n|\beta',-\mathbf{k}_2+\mathbf{Q}\rangle\langle n'|\alpha\mathbf{k}_2\rangle C^{mn}_{m'n'}(\mathbf{Q}). \tag{2.17}$$

We then make the ansatz that $C^{mn}_{m'n'}$ depends on $\mathbf{Q}$ but not on $\mathbf{k}_1$ and $\mathbf{k}_2$; the entire $\mathbf{k}_1$ and $\mathbf{k}_2$ dependence of $C^{\beta\beta'}_{\alpha'\alpha}(\mathbf{k}_1,\mathbf{k}_2,\mathbf{Q})$ originates from the overlap matrix elements of Eq. (2.17). The internal consistency of this ansatz can be demonstrated by substituting Eq. (2.17) in (2.16), which produces an algebraic equation for $C^{mn}_{m'n'}$ that is more tractable than the original integral equation:

$$C^{mn}_{m'n'}(\mathbf{Q}) = u_0\delta_{mn}\delta_{m'n'} + \sum_{l,l'}U^{ml}_{m'l'}(\mathbf{Q})C^{ln}_{l'n'}(\mathbf{Q}), \tag{2.18}$$

where

$$U^{ml}_{m'l'}(\mathbf{Q}) = u_0\int\frac{d^3k}{(2\pi)^3}G^A_{ml}(\mathbf{k})G^R_{m'l'}(-\mathbf{k}+\mathbf{Q}) \tag{2.19}$$

and

$$G^{R(A)}_{ml}(\mathbf{k}) = \sum_{\alpha} \langle m|\alpha\mathbf{k}\rangle G^{R(A)}_{\alpha}(\mathbf{k})\langle\alpha\mathbf{k}|l\rangle. \tag{2.20}$$

In matrix language, Eq. (2.18) can be rewritten as

$$\hat{C} = (\mathbf{1}_{16} - \hat{U})^{-1}\hat{C}^{(0)}, \tag{2.21}$$

where $\hat{C}^{(0)} = u_0\mathbf{1}_{16}$. Once we obtain $C^{mn}_{m'n'}$, we use Eq. (2.17) in order to recover $C^{\beta\beta'}_{\alpha'\alpha}$. During this operation, we neglect $\mathbf{Q}$ in the overlap matrix elements, which is a good approximation because $\delta\sigma$ is dominated by elements of $C^{mn}_{m'n'}(\mathbf{Q})$ that are strongly peaked at $Q \simeq 0$.

For ϵ_F in the conduction band, we once again limit ourselves to $\alpha,\beta,\alpha',\beta' \in \{1,2\}$ in Eq. (2.15). Then, we can approximate $\mathbf{k} \simeq \mathbf{k}_F$ inside the cooperon, and an integration over $|\mathbf{k}|$ yields

$$\delta\sigma_1 \simeq -6\frac{e^2}{\hbar^2}\nu D\tau\tau_0\frac{1}{W}\int\frac{d^2Q}{(2\pi)^2}\overline{C}(\mathbf{Q}), \tag{2.22}$$

where

$$\overline{C}(\mathbf{Q}) \equiv \int\frac{d\Omega_{\mathbf{k}}}{4\pi}\hat{\mathbf{k}}_x^2\sum_{\alpha,\alpha'=1,2} C^{\alpha\alpha'}_{\alpha'\alpha}(\mathbf{k}_F,\mathbf{k}_F,\mathbf{Q}) \tag{2.23}$$

and $d\Omega_{\mathbf{k}}$ is the differential solid angle subtended by $\hat{\mathbf{k}}$.

Note that $\delta\sigma_1$ depends on the lifetime τ_0 of Bloch states as well as on the transport relaxation time τ. As mentioned above, the difference between τ and τ_0 comes from the momentum dependence of $|\alpha\mathbf{k}\rangle$ states. At any rate, the full correction $\delta\sigma$ depends only on τ due to the additional contribution from $\delta\sigma_2$ [see Fig. 2(c) and Eq. (B1)]. Equation (B1) can be evaluated using the same procedure as for $\delta\sigma_1$. For instance, in Appendix B we derive

$$\delta\sigma_2 \simeq \begin{cases} 0 & \text{if } (\epsilon_F - M)/M \ll 1, \\ -(1/3)\delta\sigma_1 & \text{if } (\epsilon_F - M)/M \gg 1. \end{cases} \tag{2.24}$$

The full form of the quantum correction, $\delta\sigma_1 + \delta\sigma_2$, depends only on the transport mean-free path τ and has (in appropriate limits) a universal magnitude [see Eqs. (2.33) and (2.35)].

C. Calculations

The road map to $\delta\sigma$ starts from a calculation of $\hat{U}$ in Eq. (2.19). In Appendix C, we derive

$$U^{ml}_{m'l'} = a\,\delta_{ml}\delta_{m'l'} + \sum_{\mu} b_\mu\,\Lambda^{\mu}_{m'l'}\delta_{ml} + \sum_{\mu} c_\mu\,\Lambda^{\mu}_{ml}\delta_{m'l'} + \sum_{\mu,\nu} d_{\mu\nu}\,\Lambda^{\mu}_{ml}\Lambda^{\nu}_{m'l'}, \tag{2.25}$$

where $\mu,\nu \in \{1,2,3,4\}$, $\Lambda^i = \sigma^i\tau^x$ for $i \in \{1,2,3\}$ and $\Lambda^4 = \mathbf{1}_2\,\tau^z$. In addition, a, b_μ, c_ν, and $d_{\mu\nu}$ are $\mathbf{Q}$-dependent coefficients, the explicit expressions of which are shown in Appendix C. With those, $\hat{U}$ is fully determined.

The next task is to get $C^{mn}_{m'n'}(\mathbf{Q})$ from Eq. (2.21). While $[\mathbf{1}_{16} - \hat{U}(\mathbf{Q})]$ can be inverted numerically, it is not possible to do so analytically for $Q \neq 0$. Since we are interested in analytical expressions, we follow an approximate three-step route.

First, we diagonalize $(\mathbf{1}_{16} - \hat{U})$ for $Q = 0$, analytically. All eigenvalues can be written in the form $\Delta_g\tau_0$, where Δ_g is the "intrinsic" cooperon gap or mass. We find that one of the eigenvalues has $\Delta_g = 0$ for any ϵ_F and M, which is a reflection of combined time-reversal symmetry and charge conservation. As we elaborate in the next section, there may be additional eigenvalues with $\Delta_g \simeq 0$ when $(\epsilon_F - M)/M \ll 1$ and $(\epsilon_F - M)/M \gg 1$. Hereafter, we refer to eigenvectors of $\Delta_g \simeq 0$ eigenvalues as gapless (or massless, or "soft") modes. Because $\Delta_g \simeq 0$ eigenvalues make $\hat{C}$ large, $\delta\sigma$ is determined mainly by soft modes.

Second, we extrapolate the $Q = 0$ case to $Q \neq 0$ perturbatively, with the objective of finding how the eigenvalues of the gapless modes depend on Q. To that end, $\delta\hat{U}(\mathbf{Q}) \equiv \hat{U}(\mathbf{0}) - \hat{U}(\mathbf{Q})$ is written in the basis that diagonalizes $\hat{U}(\mathbf{0})$. The shift of $Q = 0$ eigenvalues under $\delta\hat{U}(\mathbf{Q})$ is then evaluated through standard second-order perturbation theory. The need to go to second order in $\delta\hat{U}$ originates from the fact that several matrix elements of $U^{mn}_{m'n'}(\mathbf{Q})$ are linear in Q (see Appendix C). When $(\epsilon_F - M)/M \ll 1$ and $(\epsilon_F - M)/M \gg 1$, perturbation theory leads to eigenvalues $(DQ^2 + \Delta_g)\tau_0$. The fact that D contains the transport time τ rather than the scattering time τ_0 is generally crucial in order to arrive at the correct result for $\delta\sigma$.

Third, we invert the diagonalized matrix, and transform its outcome to the $|m,m'\rangle$ basis by using the $Q = 0$ eigenvector matrix [the change of unperturbed eigenvectors under $\delta\hat{U}(\mathbf{Q})$ is deemed unimportant]. This yields $C^{mn}_{m'n'}(\mathbf{Q})$.

Once we have $C^{mn}_{m'n'}(\mathbf{Q})$, we use Eq. (2.17) in order to extract $C^{\alpha\beta}_{\beta\alpha}(\mathbf{k},\mathbf{k}',\mathbf{Q})$. This is then plugged in Eqs. (2.22) and (B1).

D. Results

The diagonalization of Eq. (2.21) at $Q = 0$ shows one genuinely gapless cooperon mode [$\Delta_g = 0$ (cf. Sec. II A)], with a spin-singlet and orbital-triplet eigenvector:

$$\left[\frac{\epsilon_F + M}{2\sqrt{\epsilon_F^2 + M^2}}|TT\rangle + \frac{\epsilon_F - M}{2\sqrt{\epsilon_F^2 + M^2}}|BB\rangle\right](|\uparrow\downarrow\rangle - |\downarrow\uparrow\rangle). \tag{2.26}$$

The fact that Eq. (2.26) remains gapless for any ϵ_F/M is a physical manifestation of charge conservation. This situation differs qualitatively from 2D TIs in HgTe quantum wells,[17] where a nonzero mass term gaps all cooperons. The reason for the difference is that in 2D TIs, the mass term acts somewhat like a Zeeman field in a 2D electron gas with Rashba spin-orbit interaction.

Importantly, the diagonalization of Eq. (2.21) reveals two qualitatively distinct regimes of quantum interference, $(\epsilon_F - M)/M \ll 1$ and $(\epsilon_F - M)/M \gg 1$, which potentially host additional gapless cooperon modes. As we discuss in the following, these additional gapless modes can change and even reverse the contribution to $\delta\sigma$ coming from Eq. (2.26).

When $(\epsilon_F - M)/M \gg 1$, we identify a slightly gapped (soft) cooperon mode with

$$\Delta_g = 2\left(M^2/\epsilon_F^2\right)\tau_0^{-1} \equiv \tau_s^{-1} \ll \tau_0^{-1}, \tag{2.27}$$

the eigenvector of which is a spin singlet and an orbital triplet:

$$\tfrac{1}{2}\left(|TB\rangle + |BT\rangle\right)\left(|\uparrow\downarrow\rangle - |\downarrow\uparrow\rangle\right). \tag{2.28}$$

Physically, τ_s^{-1} is the rate of "intervalley" transitions ($|T\rangle + |B\rangle \to |T\rangle - |B\rangle$) induced by the "mass term" ($M\tau^z$) in Eq. (2.1). Because both Eqs. (2.26) and (2.28) are spin singlets, their contributions to $\delta\sigma$ are of WAL type (this is proven in the following).

Incidentally, $M = 0$ is the physically relevant regime for time-reversal symmetric Weyl semimetals, which have two degenerate Dirac points with linear energy dispersion along the three momenta axes. Unlike in graphene,[20] where there are four gapless cooperon modes (in absence of atomically sharp defects and hexagonal warping), in a Weyl semimetal we obtain only two gapless cooperon modes. This difference stems from the fact that the SU(2) "valley symmetry" of graphene[20] gets reduced to a U(1) symmetry in Weyl semimetals, due to the band dispersion along z. Acting somewhat like a Zeeman field would in a free electron gas, the k_z dispersion generates a mass for orbital-singlet modes, which is why the nearly gapless cooperons in Eqs. (2.26) and (2.28) are orbital triplets.

When $(\epsilon_F - M)/M \ll 1$, there are three soft modes with gap

$$\Delta_g = (2/9)(1 - M/\epsilon_F)^2\tau_0^{-1} \equiv \tau_v^{-1} \ll \tau_0^{-1}. \quad (2.29)$$

Physically, τ_v^{-1} is the rate of spin-flip transitions induced by the "spin-orbit term" ($v\mathbf{k}\cdot\boldsymbol{\sigma}\tau^x$) in Eq. (2.1). The eigenvectors for the three slightly gapped modes are

$$\begin{aligned} &(\lambda_1|TT\rangle + \lambda_2|BB\rangle)|\downarrow\downarrow\rangle, \\ &(\lambda_1|TT\rangle + \lambda_2|BB\rangle)|\uparrow\uparrow\rangle, \\ &(\lambda_3|TT\rangle + \lambda_4|BB\rangle)(|\uparrow\downarrow\rangle + \downarrow\uparrow\rangle), \end{aligned} \quad (2.30)$$

where $\lambda_1, \ldots, \lambda_4$ are coefficients that depend only on ϵ_F/M, such that $\lambda_1 \simeq \lambda_3 \simeq 1 + O[(\epsilon_F/M - 1)^2]$ and $\lambda_2 \simeq \lambda_4 \simeq O[(\epsilon_F/M - 1)]$. Therefore, the three soft modes in Eq. (2.30) are all spin and orbital triplets. As will be demonstrated momentarily, their contribution to $\delta\sigma$ is of WL type.

Next, we determine $\overline{C}$ [cf. Eq. (2.23)] by diagonalizing Eq. (2.18) at $Q \neq 0$ and doing the angular integration in Eq. (2.23). For $(\epsilon_F - M)/M \ll 1$, we obtain

$$\overline{C} \simeq \frac{\hbar}{6\pi\nu\tau^2}\left[-\frac{1}{DQ^2 + \tau_\phi^{-1}} + \frac{3}{DQ^2 + \tau_\phi^{-1} + \tau_s^{-1}}\right]. \quad (2.31)$$

For $(\epsilon_F - M)/M \gg 1$, we instead get

$$\overline{C} \simeq \frac{3\hbar}{8\pi\nu\tau^2}\left[-\frac{1}{DQ^2 + \tau_\phi^{-1}} - \frac{1}{DQ^2 + \tau_\phi^{-1} + \tau_v^{-1}}\right]. \quad (2.32)$$

In the derivation of Eqs. (2.31) and (2.32), we have included the phase relaxation time τ_ϕ and exploited $DQ^2\tau_0 \ll 1$.

The first term in the square brackets of Eqs. (2.31) and (2.32) is large at $Q \to 0$ irrespective of ϵ_F/M, and originates from the spin-singlet cooperon mode in Eq. (2.26). Its negative sign means that it makes a contribution towards WAL. Equation (2.31) displays a competition between WL and WAL, which is no different from that found in an ordinary metal with spin-orbit interactions. WL terms originate from the three spin-triplet modes of Eq. (2.30). WL prevails if $\tau_\phi^{-1} \gg \tau_s^{-1}$, whereas WAL rules if $\tau_\phi^{-1} \ll \tau_s^{-1}$.

Equation (2.32) unveils two different regimes of WAL. On one hand, if $\tau_\phi^{-1} \gg \tau_v^{-1}$, the spin-singlet cooperon mode of Eq. (2.28) makes a contribution to $\delta\sigma$ that equals that of Eq. (2.26). In this limit, quantum interference can be interpreted as coming from two identical and nearly decoupled Dirac valleys. On the other hand, if $\tau_\phi^{-1} \ll \tau_v^{-1}$, the contribution from Eq. (2.28) becomes relatively unimportant and the magnitude of WAL is halved. In other words, when the intervalley transition rate induced by the mass term $M\tau^z$ is fast compared to the phase relaxation rate, the two valleys contribute as one. This is quite different from graphene, where strong intervalley scattering changes WAL into WL.[20] The underlying reason for such a qualitative difference is that in graphene a gapless valley-singlet mode is responsible for producing WL, whereas in a Weyl semimetal the valley-singlet cooperons are strongly gapped by the k_z band dispersion.

Substituting Eqs. (2.31) and (2.32) in Eq. (2.24) and doing the Q integral, we arrive at

$$\delta G \simeq \alpha\, G_q \ln(\tau_\phi/\tau), \qquad \alpha = \begin{cases} -1 & \text{if } \tau_\phi \ll \tau_s, \\ 1/2 & \text{if } \tau_\phi \gg (\tau_v, \tau_s), \\ 1 & \text{if } \tau_\phi \ll \tau_v, \end{cases} \quad (2.33)$$

where $\delta G \equiv W\delta\sigma$ is the quantum interference correction to *conductance* and

$$G_q \equiv e^2/(2\pi^2\hbar) \quad (2.34)$$

is a universal conductance unit. In the derivation of Eq. (2.33), we have used Eq. (2.24). The reason why $\alpha = 1/2$ when $\tau_\phi \gg (\tau_v, \tau_s)$ is that in such regime there is only one gapless cooperon mode (hence $|\alpha| = 1/2$), which is a spin singlet (hence $\alpha = |\alpha|$).

While Eq. (2.33) is valid in the absence of external magnetic fields, the magnetoconductance $\Delta G(H) \equiv G(H) - G(0) \simeq \delta G(H) - \delta G(0)$ can be easily obtained from Eq. (2.33) for H perpendicular to the TI thin film. The replacement of $\int d^2Q$ by an appropriate sum over Landau levels[15] results in

$$\Delta G \simeq \alpha\, G_q f(H_\phi/H), \qquad \alpha = \begin{cases} -1 & \text{if } \tau_H \ll \tau_s, \\ 1/2 & \text{if } \tau_H \gg (\tau_v, \tau_s), \\ 1 & \text{if } \tau_H \ll \tau_v, \end{cases} \quad (2.35)$$

where $f(z) \equiv \ln z - \psi(1/2 + z)$ with asymptotes $f(z) \propto z^{-2}$ for $z \gg 1$ and $f(z) \propto \ln(1/z)$ for $z \ll 1$, ψ is the digamma function,

$$\tau_H^{-1} \equiv \tau_\phi^{-1} + 2eDH/\hbar \quad \text{and} \quad H_\phi \equiv \hbar/(4eD\tau_\phi). \quad (2.36)$$

Three conclusions of experimental relevance can be extracted from Eqs. (2.33) and (2.35), which apply when highest-occupied electronic states are all located near the Γ point. First, bulk TI bands can display $\alpha = -1$ (WL) as long as the chemical potential is sufficiently close to the bottom of the bulk conduction band. Second, bulk TI bands can produce $\alpha = 1$ when ϵ_F/M is sufficiently large. Third, when $(\epsilon_F - M)/M$ is neither large nor small, $\alpha = 1/2$ ensues; this

is the conventional result expected for ordinary conducting thin films with strong spin-orbit coupling, and is the one that has been often presumed in experiments on TI films.[6–11] At $\tau_H \simeq \tau_s$, there is a crossover between $\alpha = -1$ and $1/2$; likewise, at $\tau_H \simeq \tau_v$ there is a crossover between $\alpha = 1/2$ and 1.

The particular expressions for τ_s and τ_v in Eqs. (2.27) and (2.29) rely on our assumption of $V_{\rm dis} \propto \mathbf{1}_4$. Spin-orbit coupled impurities and/or atomically sharp disorder potentials would induce additional spin- and valley-flip processes, the rates τ_{sf}^{-1} and τ_{vf}^{-1} of which would have to be incorporated via $\tau_s^{-1} \to \tau_s^{-1} + \tau_{sf}^{-1}$ and $\tau_v^{-1} \to \tau_v^{-1} + \tau_{vf}^{-1}$. If τ_{vf}^{-1} and τ_{sf}^{-1} are strong enough and insensitive to the value of ϵ_F/M, then the only surviving regime of interference corrections is the conventional $\alpha = 1/2$.

The conventional $\alpha = 1/2$ can be found in a wide range of parameter space at low temperatures, whereas the unconventional $\alpha = -1$ and 1 emerge in the relatively narrow regimes $\tau \ll \tau_H \ll \tau_s$ and $\tau \ll \tau_H \ll \tau_v$ (respectively). How accessible are these unconventional regimes? Suppose $M \simeq 150$ meV, $v \simeq 5 \times 10^5$ m/s, and a bulk carrier density of $n \simeq 3 \times 10^{18}$ cm^{-3}. This situation corresponds to having a small bulk Fermi surface. Then, it follows that $\alpha \simeq -1$ for a fairly wide range of magnetic fields $(l_H/(12l) \ll 1$, where $l_H \equiv (D\tau_H)^{1/2})$. The limit $\alpha \to 1$ is not accessible in this regime. Instead, $\alpha \simeq 1$ should be accessible in (i) Weyl semimetals or in TIs with very narrow band gaps, (ii) in TIs with large band gap but $M(\mathbf{k}_F) \simeq 0$. For the latter case, it must be kept in mind that in the absence of spherical symmetry, $M(\mathbf{k}_F)$ is not constant on the Fermi surface. Suppose $M \simeq 5$ meV and a bulk carrier density of $\simeq 2 \times 10^{18}$ cm^{-3}. Then, $\alpha \simeq 1$ in the range of fields corresponding to $l_H/(10l) \ll 1$. For typical thin films, the requirements for $\alpha = \pm 1$ are compatible with $k_F l \gg 1$. Materials such as $BiTl(S_{1-\delta}Se_\delta)_2$, where controlled changes of δ can tune M from 0 to large values,[23] appear to be good candidates to observe crossovers between different regimes of magnetoresistance in Eq. (2.35).

Our analysis has thus far neglected surface states of the TI, which can also contribute to the measured magnetoresistance. It can be argued that surface states are unimportant and Eq. (2.35) suffices in trivial insulators described by Eq. (2.1), as well as in time-reversal-invariant Weyl semimetals and in TIs with very small bulk band gaps ($\lesssim \hbar/\tau_0$). In contrast, when the surface states of the TI are robust, Eq. (2.35) is incomplete and must be generalized. Such generalization is the subject for the rest of this paper.

III. QUANTUM CORRECTIONS TO CONDUCTIVITY FROM COUPLED BULK AND SURFACE STATES

In this section, we consider the combined bulk-surface contribution to $\delta\sigma$ in 3D TIs with relatively large band gaps. We concentrate on a particular setup that consists of a TI thin film gated on one surface. The gate voltage can produce a depletion layer that spatially separates bulk and surface carriers (Fig. 9), and carriers tunnel back and forth across the depletion layer. We assume the bulk-surface tunneling rate to be much smaller than the elastic scattering time on either side of the depletion layer, so that electrons scatter many times within the bulk (surface) before tunneling to the surface (bulk). This assumption is experimentally realistic, and it simplifies the microscopic theory of this section considerably.

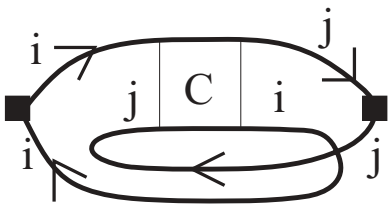

FIG. 3. Diagrammatic representation for $\delta\sigma_{ij}$, where i and j are layer indices. For 2D layers without spin-orbit coupling, the cooperon matrix elements are fully characterized by layer indices. The velocity operator is diagonal in the layer index; therefore, the cooperons C_{22}^{11} and C_{11}^{22} do not enter in the expression for $\delta\sigma_{ij}$.

A. Single isolated TI surface

As a preliminary step, we recall the expression for $\delta\sigma$ on a single TI surface that is decoupled from the bulk. Taking $\epsilon_{Fs}\tau \gg 1$, where ϵ_{Fs} is the Fermi energy measured from the Dirac point of the surface states, one arrives[16,17] at

$$\Delta G/G_q = (1/2) f(H_\phi/H) \tag{3.1}$$

for any τ_H. The prefactor $1/2$ is consistent with having a gapless spin-singlet cooperon (the spin-triplet cooperons have large gaps due to the strong spin-momentum coupling on the surface).

B. Two coupled 2D layers without spin-orbit coupling

As another preliminary step, here we compute $\delta\sigma$ for two ordinary metallic 2D layers separated by a tunnel barrier. In a double-layer system, the current flowing in layer i can be written as $\mathbf{j}_i = \sum_j \sigma_{ij}\mathbf{E}_j$, where $\mathbf{E}_j$ is the electric field in layer j. For concreteness, we take $\mathbf{E}_1 = \mathbf{E}_2 \equiv \mathbf{E}$, so that the measured current is $\mathbf{j} = \mathbf{j}_1 + \mathbf{j}_2 = \sigma\mathbf{E}$ with $\sigma = \sum_{ij}\sigma_{ij}$. Consequently, the quantum corrections to conductivity are $\delta\sigma = \sum_{ij}\delta\sigma_{ij}$. The goal of this section is to compute $\delta\sigma$ from microscopic theory.

The interference correction $\delta\sigma_{ij}$ has the diagrammatic representation shown in Fig. 3. Because the velocity operator is diagonal in the layer index, the only cooperons that enter in the conductivity are C_{ji}^{ij}, with $i,j \in \{1,2\}$. In particular, $\delta\sigma_{ii}$ involves intralayer cooperons C_{ii}^{ii}, whereas $\delta\sigma_{12}$ and $\delta\sigma_{21}$ involve interlayer cooperons C_{21}^{12} and C_{12}^{21} (Fig. 4). Assuming that disorder potentials in the two layers are uncorrelated,

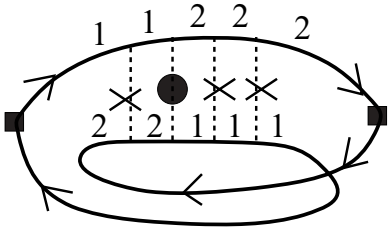

FIG. 4. Typical microscopic process that gives rise to $\delta\sigma_{12}$. It can be neglected when the intralayer disorder potentials in the two layers are uncorrelated.

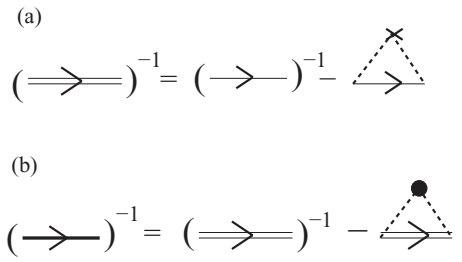

FIG. 5. Single-particle Green's functions. (a) Dressing of Bloch states due to intralayer impurity scattering. (b) Dressing of disorder-averaged Green's functions due to interlayer tunneling. The tunneling amplitude is regarded as a random variable.

$C^{ij}_{ji} = 0$ for $i \neq j$. This is a reasonable assumption when electrons in the two layers scatter off different sets of impurities. Hence, we are left with $\delta\sigma = \sum_i \delta\sigma_{ii}$. From here on, we simplify the notation via $C^{ii}_{ii} \equiv C_i$.

When evaluating $\delta\sigma_{ii}$ we will neglect spin-orbit interactions; however, the main lessons learned in this section will be transferrable to the spin-orbit coupled case studied in the next section. In absence of interlayer coupling, a standard calculation yields

$$\delta\sigma^{(0)}_{ii} \simeq -4\frac{e^2}{\hbar^2}\nu_i D_i \tau_{di}^2 \int_{\mathbf{Q}} C^{(0)}_i(\mathbf{Q}), \tag{3.2}$$

where $\int_{\mathbf{Q}} \equiv \int d^2Q/(2\pi)^2$, an extra factor of 2 is due to spin degeneracy, τ_{di} is the scattering time in layer i due to elastic impurities (we assume purely s-wave scattering, so that there is no difference between the transport scattering time and the quantum lifetime), ν_i is the density of states per unit area in layer i, and

$$C^{(0)}_i(\mathbf{Q}) = \frac{\hbar}{2\pi\nu_i\tau_{di}^2}\frac{1}{D_i Q^2 + \tau_{\phi i}^{-1}} \tag{3.3}$$

is the cooperon for an isolated layer. In presence of interlayer tunneling, $C^{(0)}_i$ in Eq. (3.2) is replaced by C_i:

$$\delta\sigma_{ii} \simeq -4\frac{e^2}{\hbar^2}\nu_i D_i \tau_{di}^2 \int_{\mathbf{Q}} C_i(\mathbf{Q}), \tag{3.4}$$

in whose prefactor we have neglected terms containing the ratio between the tunneling rate and the elastic scattering rate.

In order to compute C_i, we recognize that the influence of interlayer coupling occurs at two different levels. On one hand, it modifies the single-particle Green's function for each layer (Fig. 5). Because the thickness of the depletion layer typically shows microscopic variations within the same film as well as from sample to sample, the interlayer tunneling amplitude can be regarded as a random variable. Consequently, the change in the ensemble-averaged Green's function due to tunneling can be captured via $\tau_{di}^{-1} \to \tau_{di}^{-1} + \tau_{ti}^{-1}$, where

$$\tau_{ti}^{-1} = (2\pi/\hbar)\langle|t|^2\rangle S\,\nu_j \tag{3.5}$$

is the tunneling rate from layer i onto layer $j \neq i$, $\langle|t|^2\rangle$ is the averaged square of the tunneling matrix element, and S is the layer area. Note that $\langle|t|^2\rangle$ scales like S^{-1}, so that τ_{ti}^{-1} is independent of the layer area.

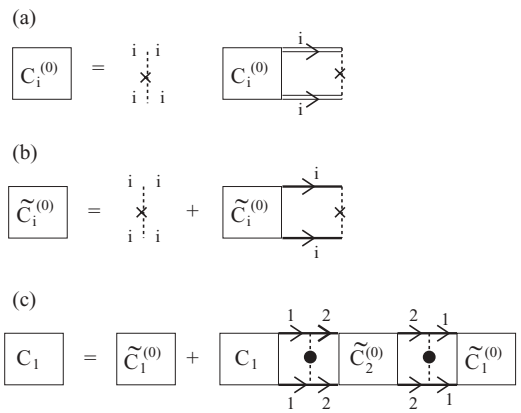

FIG. 6. (a) Cooperon $C^{(0)}_i$ without interlayer tunneling. (b) Partially dressed cooperon $\tilde{C}^{(0)}_i$, where tunneling is included solely in the single-particle Green's functions. $\tilde{C}^{(0)}_i$ can be directly obtained from $C^{(0)}_i$ via $\tau_{\phi i} \to \tilde{\tau}_{\phi i}$. (c) Fully dressed cooperon C_i, where tunneling is incorporated both in the single-particle Green's function and in the particle-particle correlations.

On the other hand, interlayer tunneling modifies particle-particle correlations that build up cooperons. An approximate diagrammatic expression for these correlations is shown in Fig. 6. The equation of Fig. 6(c) can be solved in momentum space and it yields

$$C_i = \frac{\hbar}{2\pi\nu_i\tau_{di}^2}\frac{D_j Q^2 + \tilde{\tau}_{\phi j}^{-1}}{\left(D_1 Q^2 + \tilde{\tau}_{\phi 1}^{-1}\right)\left(D_2 Q^2 + \tilde{\tau}_{\phi 2}^{-1}\right) - \tau_{t1}^{-1}\tau_{t2}^{-1}} \tag{3.6}$$

for $j \neq i$. In the derivation of Eq. (3.6), we have introduced

$$\tilde{\tau}_{\phi i}^{-1} \equiv \tau_{\phi i}^{-1} + \tau_{ti}^{-1} \tag{3.7}$$

as an effective phase relaxation rate that incorporates tunneling, and have used

$$\int_{\mathbf{k}} G^R_i(\mathbf{k}) G^A_i(-\mathbf{k}+\mathbf{Q}) \simeq \frac{2\pi\nu_i\tau_{di}}{\hbar}\left(1 - \frac{\tau_{di}}{\tilde{\tau}_{\phi i}} - D_i Q^2 \tau_{di}\right).$$

Microscopic processes depicted in Fig. 6 leave out those in which two consecutive tunneling events occur without any intralayer scattering in-between. Likewise, they ignore electron trajectories in which a tunneling event precedes any intralayer scattering (Fig. 7). These processes are relatively unimportant if $\tau_{ti} \gg \tau_{di}$. Not surprisingly, Eq. (3.6) arises in the coupled equations for the classical diffusive conductivity as well (see Appendix D).

FIG. 7. Typical processes not included in Fig. 6, as they are subdominant for $\tau_{ti} \gg \tau_{di}$.

It is convenient to rewrite C_i in Eq. (3.6) as

$$C_i = \frac{\hbar}{2\pi \nu_i D_i \tau_{di}^2}\left[\frac{A_i}{Q^2+q_a^2}+\frac{B_i}{Q^2+q_b^2}\right], \tag{3.8}$$

where

$$2q_{a(b)}^2 = \frac{1}{\tilde{l}_{\phi 1}^2}+\frac{1}{\tilde{l}_{\phi 2}^2} \pm \sqrt{\left(\frac{1}{\tilde{l}_{\phi 1}^2}-\frac{1}{\tilde{l}_{\phi 2}^2}\right)^2+\frac{4}{l_{t1}^2 l_{t2}^2}} \tag{3.9}$$

and

$$A_i = 1 - B_i = \left(\tilde{l}_{\phi j}^{-2} - q_a^2\right)/\left(q_b^2 - q_a^2\right) \quad \text{for } j \neq i. \tag{3.10}$$

In Eq. (3.9), we have defined $\tilde{l}_{\phi i} \equiv (D_i \tilde{\tau}_{\phi i})^{1/2}$ as an effective coherence length and $l_{ti} \equiv (D_i \tau_{ti})^{1/2}$ as the interlayer leakage length. Besides, q_a^2 (q_b^2) gets the positive (negative) sign in front of the square root. Combining Eq. (3.4) with Eq. (3.8) and using $A_1 + A_2 = B_1 + B_2 = 1$, we get

$$\delta\sigma = \sum_i \delta\sigma_{ii} = -2\frac{e^2}{\pi\hbar}\int_{\mathbf{Q}}\left[\frac{1}{Q^2+q_a^2}+\frac{1}{Q^2+q_b^2}\right]. \tag{3.11}$$

Therefore, the low-field magnetoconductance reads as

$$\Delta\sigma = \sum_i \Delta\sigma_{ii} = -G_q\left[f\left(\frac{H_a}{H}\right)+f\left(\frac{H_b}{H}\right)\right], \tag{3.12}$$

where

$$H_{a(b)} \equiv \hbar\, q_{a(b)}^2/(4e). \tag{3.13}$$

In the limit of very strong tunneling ($\tau_{ti}/\tau_{\phi i} \to 0$), Eq. (3.12) becomes $\Delta\sigma \simeq -G_q f(H_b/H)$, as though there was a single layer. In the limit of very weak tunneling ($\tau_{ti}/\tau_{\phi i} \to \infty$), $\Delta\sigma$ is the sum of contributions from two independent films.

It is helpful to understand the weak- and strong-coupling regimes in terms of measurable quantities such as the interlayer conductance per square

$$g_t = (2\pi e^2/\hbar)\langle|t|^2\rangle S \nu_1 \nu_2 = \sigma_{Di}/l_{ti}^2, \tag{3.14}$$

where σ_{Di} is the Drude conductivity in layer i. For simplicity, suppose that $\tau_{\phi 1} \simeq \tau_{\phi 2} \equiv \tau_\phi$. In this case, the crossover from weak to strong tunneling occurs when

$$\frac{1}{g_t l_\phi^2} \lesssim \frac{1}{\sigma_{D1}}+\frac{1}{\sigma_{D2}} \quad \text{(crossover condition)}, \tag{3.15}$$

namely, when the tunneling resistance for a square of area l_ϕ^2 becomes smaller than the sum of the classical intralayer resistivities. Let us define

$$g_c^{-1} \equiv \left(\sigma_{D1}^{-1}+\sigma_{D2}^{-1}\right) l_\phi^2. \tag{3.16}$$

If $g_t \ll g_c$, then $\Delta\sigma/G_q \simeq -2\ln(H/H_\phi)$ for $H \gg H_\phi$. If $g_t \gg g_c$, then $\Delta\sigma/G_q \simeq -\ln(H/H_\phi)$ for $H_\phi \ll H \ll H_\phi(g_t/g_c)$. Thus, changing the interlayer conductance results in a factor-of-2 change for the magnitude of the WL correction.

Limits reminiscent of the above were first discussed in inversion layers of multivalley semiconductors such as Si,[24] where the role of the layers is played by different electron pockets in the Brillouin zone. Similarities notwithstanding, there are clear differences between our microscopic theory and that of multivalley semiconductors. On one hand, the separation in momentum between valleys of Si prevents scattering processes such as the one in Fig. 8. These processes are not only allowed in our case, but also lead to the cooperon dressing shown in Fig. 6(c). On the other hand, in our case, the interlayer cooperon vanishes due to uncorrelated disorder potentials in the two spatially separated layers. That is not the case in multivalley semiconductors, where both valleys scatter off the same set of real-space impurities and intervalley cooperons contribute crucially to $\delta\sigma$.

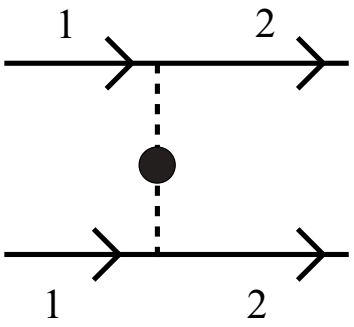

FIG. 8. Example of an interlayer scattering process that is allowed in multilayer systems. Its analog in multivalley semiconductors of Ref. 24 is forbidden.

Finally, it should be mentioned that Eqs. (3.9), (3.10), and (3.12) coincide with those derived by Bergmann,[25] who invoked macroscopic arguments based on the diffusion equation. The microscopic theory of this section supports Bergmann's results, insofar as $\tau_{ti} \gg \tau_{di}$ and the disorder potentials in the two layers are uncorrelated. Incidentally, yet another way to arrive at the same results is unveiled in Appendix E; this later method will prove convenient in the upcoming section.

C. 3D TI film with bulk-surface coupling

We now consider a 3D TI film (Fig. 9) with a gate electrode placed near its top surface. At the moment, we neglect the

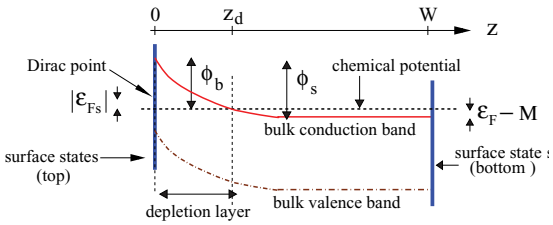

FIG. 9. (Color online) Schematic energy band profile for a gated 3D TI thin film. $z = 0$ corresponds to the top surface of the device, immediately under the gate. $z = W$ corresponds to the bottom (ungated) surface. The vertical (blue) solid lines at $z = 0, W$ are surface states. The curved solid (red) line is the bulk conduction band, and the dotted-dashed (brown) curve is the bulk valence band. The chemical potential is depicted by a horizontal dashed line. z_d is the thickness of the depletion layer, where neither bulk nor surface carriers are present. ϵ_{Fs} is the Fermi energy of the surface states measured from the Dirac point ($\epsilon_{Fs} < 0$ in this figure). ϵ_F is the Fermi energy of the bulk states, measured with respect to the midgap point.

bottom surface of the TI, which will be incorporated below. For ease of notation, we use subscript "1" to refer to "bulk" and subscript "2" to refer to "top surface." As in the preceding section, we assume bulk-surface disorder correlations to be negligible, so that the quantum corrections to conductance can be written as $\delta G = \delta G_{11} + \delta G_{22} = W\delta\sigma_{11} + \delta\sigma_{22}$. δG is approximately independent of the film thickness W as long as $W \ll \tilde{l}_{\phi 1}$, where $\tilde{l}_{\phi 1}$ was defined below Eq. (3.10).

The goal of this section is to calculate δG from microscopic theory. Unlike in the previous section, here both "layers" are spin-orbit coupled. We assume that tunneling events, albeit being time-reversal invariant, conserve neither spin nor orbital degrees of freedom. Indeed, in a TI, spin is not conserved for non-momentum-conserving tunneling. Similarly, the orbital degree of freedom is not conserved due to broken inversion symmetry near the surface.

Let us begin with no tunneling. On one hand, there are four surface cooperon modes: one gapless spin-singlet mode and three spin-triplet modes with large ($\sim \tau_{d2}^{-1}$) gaps. On the other hand, there are 16 bulk cooperons, of which a spin-singlet mode [Eq. (2.26)] is always gapless. In addition, four of the bulk modes [the spin singlet of Eq. (2.28) and three spin triplets of Eq. (2.30)] can be "soft" depending on ϵ_F/M. The rest of the bulk cooperon modes have large gaps of order τ_{d1}^{-1}.

Let us now turn on tunneling. Since $\tau_{ti} \gg \tau_{di}$, we can limit ourselves to analyzing the effects of tunneling within the low-energy subspace formed by the soft cooperons. If there are no magnetic impurities in the depletion layer, the total spin of the cooperon is a good quantum number even in presence of tunneling. Accordingly, tunneling does not mix spin-singlet modes with spin-triplet modes, and the full (dressed) cooperons can also be classified into spin singlets and a spin triplet.

In the regimes $\tau_{\phi 1} \ll \tau_s$ and $\tau_{\phi 1} \gg (\tau_s, \tau_v)$, tunneling dresses one soft spin-singlet cooperon in the bulk with another soft spin-singlet cooperon on the surface. This dressing is completed as explained in Sec. III B: first by renormalizing the phase relaxation time $\tau_{\phi i} \to \tilde{\tau}_{\phi i}$, and afterwards proceeding with the series expansion of Fig. 6(c). All "blocks" appearing in this series expansion are spin singlets. When $\tau_{\phi 1} \ll \tau_s$, the soft spin-triplet cooperons from the bulk are dressed simply through $\tau_{\phi 1} \to \tilde{\tau}_{\phi 1}$: they do not get appreciably admixed with the spin-triplet cooperon on the surface because the latter has a large gap.

In the regime $\tau_{\phi 1} \ll \tau_v$, there are two gapless singlet cooperons in the bulk, each of which can hybridize with the singlet gapless cooperon on the surface. For this situation, Fig. 6(c) does not capture all possible processes and the calculation from the previous section must be generalized; this generalization is carried out in Appendix E.

With the above considerations in mind, we combine Eqs. (2.35) and (3.1) in order to obtain the total contribution to low-field magnetoconductance:

$$\frac{\Delta G}{G_q} \simeq \frac{1}{2}\begin{cases} f\left(\frac{H_a}{H}\right) + f\left(\frac{H_b}{H}\right) - 3f\left(\frac{\tilde{H}_{\phi 1}}{H}\right) & \text{if } \tilde{\tau}_H \ll \tau_s, \\ f\left(\frac{H_a}{H}\right) + f\left(\frac{H_b}{H}\right) & \text{if } \tilde{\tau}_H \gg (\tau_s, \tau_v), \\ f\left(\frac{H_c}{H}\right) + f\left(\frac{H_d}{H}\right) + f\left(\frac{\tilde{H}_{\phi 1}}{H}\right) & \text{if } \tilde{\tau}_H \ll \tau_v, \end{cases} \tag{3.17}$$

where $H_l = \hbar\, q_l^2/(4e)$ for $l \in \{a,b,c,d\}$,

$$\tilde{H}_{\phi 1} \equiv \hbar/(4eD_1\tilde{\tau}_{\phi 1}), \text{ and } \tilde{\tau}_H^{-1} \equiv \tilde{\tau}_{\phi 1}^{-1} + 2eD_1H/\hbar. \tag{3.18}$$

Note that the effective phase relaxation rate increases linearly with the bulk-to-surface tunneling rate [cf. Eq. (3.7)]. The characteristic momenta $q_{a(b)}$ have been introduced earlier in Eq. (3.9). The additional momenta $q_{c(d)}$ are identical to $q_{a(b)}$, except for $\tau_{t2}^{-1} \to 2\,\tau_{t2}^{-1}$. The reason for this difference is that the surface cooperon can decay into two gapless bulk cooperons when $\tau_{\phi 1} \ll \tau_v$.

The first line of Eq. (3.17) displays a competition between WL and WAL, and suggests that it is possible to induce a WAL-to-WL transition with a varying gate voltage. In the weak-tunneling regime WL prevails, whereas in the strong-tunneling regime WAL takes over. Similarly, a gate voltage can induce transitions between three different WAL coefficients: $\alpha \in (1/2,1)$ in the second line, and $\alpha \in (1/2,3/2)$ in the third line. The second line of Eq. (3.17) describes quantum corrections as if they originated from two independent thin films with mixed bulk-surface character; indeed, universal results expected for the simplectic symmetry class are recovered when the effective phase relaxation times become the longest time scales of the problem. Some simple limiting cases of Eq. (3.17) are discussed in Appendix F.

Thus far, we have considered the coupling between the bulk and *one* (the top) surface of the TI film. As a consequence, Eq. (3.17) applies to a TI film only if the phase relaxation time of the bottom surface (adjacent to the substrate) is short compared to other phase relaxation and tunneling times in the problem. This condition is likely not met in some recent experiments,[7,10] which report on independent contributions from both surfaces. Partly motivated by these experiments, we now generalize Eq. (3.17) so as to capture two surfaces, each coupled to bulk states.

We consider the scenario depicted in Fig. 9, where the bottom surface contains bulk carriers. Since there is no depletion layer near $z = W$, we assume that the bulk-surface tunneling rate therein is strong compared to the phase relaxation rate, yet weak compared to disorder scattering rate. Hence, we describe the hybrid of bottom surface and bulk states via Eq. (F1), and thereafter couple this hybrid to the top surface along the lines of Eq. (3.17). The resulting expression for ΔG can be approximated as

$$\frac{\Delta G}{G_q} \simeq \frac{1}{2} f\left(\frac{H'_a}{H}\right) + \frac{1}{2} f\left(\frac{H'_b}{H}\right), \tag{3.19}$$

where $H'_{a(b)} \equiv \hbar(q'_{a(b)})^2/(4e)$. The characteristic momenta q'_a and q'_b obey Eq. (3.9), where "1" labels the top surface and "2" labels a hybrid between the bottom surface and the bulk.

Notably, Eq. (3.19) implies that WL is no longer possible once the bottom surface is strongly coupled to bulk states. Instead, conventional WAL ensues with $\alpha \in (1/2,1)$. This observation not only sheds light on why current experiments see no indication for WL, but it also gives insight as to how WL could be observed in TI films.

A possible strategy is to degrade the surfaces, e.g., by depositing magnetic impurities on them, and decoupling them from the bulk by double-sided gating. One may expect WL even if only the top surface is decoupled, while the (degraded)

bottom surface is in contact with the bulk. In this case, Eq. (3.17) reduces to Eq. (2.35) derived for the sole bulk conduction, with the replacement $\tau_{\phi 1}^{-1} \to \tau_{\phi 1}^{-1} + \tau_{t3}^{-1}$, where τ_{t3} is the tunneling rate of electrons from bulk to the bottom surface. If the film is thick enough, then τ_{t3}^{-1} may become sufficiently small to provide some dynamic range for observing WL behavior. This same strategy can also facilitate the observation of WAL with $\alpha > 1$.

D. Estimates for the bulk-surface coupling

This section is devoted to an approximate electrostatic and quantum mechanical analysis of the depletion layer in a TI film, which will result in quantitative estimates for the bulk-surface coupling.

For a TI with an n-doped bulk, a negative charge per unit area $(-Q_g)$ placed at the gate repels electrons from bulk bands at $z = 0$ as well as from the surface states at $z = 0$. This leaves a positive net charge on the top surface, which is equivalent to a downward shift in the local chemical potential at $z = 0$: $\Delta\mu_s = \epsilon_F - \epsilon_{Fs}$. Recall that ϵ_{Fs} is the Fermi energy of the surface states measured from the Dirac point (for simplicity, the Dirac point is assumed to be in the middle of the band gap at $z = 0$) and ϵ_F is the Fermi energy of the bulk states measured from the middle of the band gap. Since the chemical potential deep inside the bulk must be unaffected by the gate, $\Delta\mu_s \neq 0$ implies a band bending of magnitude $\phi_s = \Delta\mu_s$ near the gated surface (Fig. 9).

When $\Delta\mu_s > (\epsilon_F - M)$, there are no bulk carriers left at $z = 0$ and a depletion layer appears at $z \in (0, z_d)$, where z_d is determined below. For each value of Q_g, $\Delta\mu_s$ (or equivalently ϵ_{Fs}) can be uniquely determined from the overall neutrality condition $Q_s + Q_d = Q_g$, where Q_s is the positive net charge induced on the surface, and Q_d is the positive net charge in the depletion layer.

In the depletion approximation,[26] one has $Q_d \simeq n z_d$, where n [cf. Eq. (2.3)] is equal to the density of charged donors in the depleted region. The electrostatic energy profile in the depleted region then obeys

$$\phi(z) = \phi_b - \frac{1}{2}\frac{e^2 n}{\kappa}(z - z_d)^2, \tag{3.20}$$

where $\phi_b \equiv \phi_s - (\epsilon_F - M) = M - \epsilon_{Fs}$, κ is the static dielectric constant, and

$$z_d = \sqrt{\frac{2\kappa\phi_b}{e^2 n}}. \tag{3.21}$$

In the derivation of Eq. (3.20), we have assumed that the electric field vanishes at $z = z_d$, which is accurate within a screening radius. As the gate voltage is made more negative, the maximum width of the depletion layer ($z_d^{\max}$) is achieved when $\phi_b \simeq 2M$. For $\phi_b > 2M$, the bulk bands get inverted at $z = 0$ and z_d saturates. We estimate $z_d^{\max} \simeq 20$ nm for some typical parameter values ($M = 150$ meV, $n \simeq 4 \times 10^{18}$ cm^{-3}, $\kappa = 50$).

Once the electrostatic profile of the TI film is characterized, we can analyze the quantum mechanical tunneling of electrons across the depletion layer. The tunneling conductance per unit area is roughly

$$g_t \sim (e^2/h)\lambda_F^{-2} \exp(-2\chi), \tag{3.22}$$

where λ_F is the smallest between bulk and surface Fermi wavelengths, and

$$\chi \simeq \int_0^{z_d} dz \frac{\phi_b - \phi(z)}{\hbar v} \simeq \frac{1}{6}\frac{e^2 n z_d^3}{\kappa \hbar v}. \tag{3.23}$$

In Eq. (3.23), we have ignored effective mass and Fermi velocity mismatches across the depletion layer. The WKB exponent χ can be tuned by a gate voltage: as z_d varies from 0 to $z_d^{\max}$, χ goes from 0 to $\simeq 6$.

Drawing from the previous section [cf. Eq. (3.15)], the crossover from weak to strong bulk-surface coupling occurs when

$$\frac{1}{g_t l_\phi^2} \lesssim \frac{1}{\sigma_{D1} W} + \frac{1}{\sigma_{D2}} \simeq \frac{1}{\sigma_{D2}}, \tag{3.24}$$

where in the second equality we have assumed that $\sigma_{D1} W \gg \sigma_{D2}$. This is a good assumption provided that (i) the bulk mean-free path is of the same order as the surface mean-free path, and (ii) $k_F W \gg 1$. Plugging Eq. (3.22) in Eq. (3.24), the latter becomes

$$\frac{l_\phi}{\lambda_F} \gtrsim (k_{Fs} l_2)^{1/2} \exp(\chi), \tag{3.25}$$

where $k_{Fs} = |\epsilon_{Fs}|/\hbar v$ is the Fermi wave vector for the surface states and we have used $\sigma_{D2} \sim (e^2/h) k_{Fs} l_2$.

When $z_d = z_d^{\max}$, the right-hand side of Eq. (3.25) reaches $\simeq 1000$, which exceeds the typical l_ϕ/λ_F in TI thin films by at least an order of magnitude. Therefore, when the depletion layer has its maximum width, the top surface and the bulk of the TI film can be regarded as weakly coupled. This state of affairs changes rapidly when the depletion layer is made thinner by a gate voltage. For instance, when $z_d = z_d^{\max}/\sqrt{2}$, the right-hand side of Eq. (3.25) equals $\simeq 30$, which is comparable to the typical l_ϕ/λ_F. Further slight reductions in z_d can subsequently drive the film into a regime of strong bulk-surface coupling. These estimates justify the interpretation of experimental data given in, e.g., Ref. 11.

IV. SUMMARY AND CONCLUSIONS

We have completed a theoretical study of low-field magnetoresistance in electrostatically gated 3D TI films. The concise analytical expressions presented here [Eqs. (2.35), (3.17), and (3.19)] may shed light on the quantum magnetoresistance of TIs, Weyl semimetals, as well as some topologically trivial materials. Only magnetic fields that are perpendicular to the TI thin film have been considered in this work; for in-plane fields and small bulk band gaps, quantum interference contributions might be masked by classical magnetoresistance anomalies.[27]

A number of predictions from this work have not been articulated in previous studies and await experimental confirmation. For instance, we find that TI thin films with low bulk doping may exhibit weak localization (WL) or negative magnetoresistance instead of the often presumed weak antilocalization (WAL) or positive magnetoresistance. Admittedly, the parameter space for WL is relatively narrow, and vanishes when either surface of the TI film is strongly coupled to bulk states. However, WL may be experimentally accessible in thicker films, or in thin films where the surfaces have short phase relaxation times. Under these conditions, a

gate can induce a crossover between WL and WAL. On a separate note, we find that the "universal" prefactor for WAL varies depending on the band gap of the TI, on the bulk doping concentration, on the phase relaxation times, and on the applied gate voltage.

The results from this work are applicable to conducting yet lightly doped TIs, with thicknesses ranging between the bulk transport mean-free path and the bulk phase relaxation length. It may be useful to find out how the results derived here change in highly doped TIs containing additional electrons pockets away from the Γ point. Likewise, it may be helpful to extend our results to thinner films. Other potentially interesting tasks involve investigating universal conductance fluctuations and determining the influence of electron-electron interactions in the magnetoresistance of doped TI films.

ACKNOWLEDGMENTS

This research has been financially supported by a fellowship from Yale University (I.G.), and by NSF DMR Grant No. 0906498 (L.G.). L.G. thanks P. Jarillo-Herrero for a discussion that initiated this work, I.G. thanks E. Hankiewicz for an informative conversation, and both authors thank A. Kapitulnik for bringing Ref. 14 to their attention.

APPENDIX A: RENORMALIZED VELOCITY OPERATOR

The velocity operators appearing in the expressions for σ_D and $\delta\sigma$ (cf. Sec. II B) must be renormalized with ladder diagrams containing impurity scattering. The Dyson equation for the renormalized velocity operator is (Fig. 10)

$$\tilde{\mathbf{v}}_{\alpha\beta}(\mathbf{k}) = \mathbf{v}_{\alpha\beta}(\mathbf{k}) + u_0 \sum_{\alpha,\beta\in\{1,2\}} \int_{\mathbf{k}'} \langle\alpha\mathbf{k}|\alpha'\mathbf{k}'\rangle\langle\beta'\mathbf{k}'|\beta\mathbf{k}\rangle G^A(\mathbf{k}') \times G^R(\mathbf{k}')\tilde{\mathbf{v}}_{\alpha'\beta'}(\mathbf{k}'), \tag{A1}$$

where $\mathbf{v}_{\alpha\beta}(\mathbf{k}) = \delta_{\alpha\beta}\hbar v^2\mathbf{k}/E_k$ is a matrix element for the bare velocity operator. We solve Eq. (A1) by guessing a solution of the form

$$\tilde{\mathbf{v}}_{\alpha\beta}(\mathbf{k}) = \gamma_k \mathbf{k}\delta_{\alpha\beta}, \tag{A2}$$

where γ_k is a scalar that depends on $|\mathbf{k}|$ but not $\hat{\mathbf{k}}$. Although it is *a priori* not obvious that the renormalized velocity operator should be diagonal in the band indices, by substituting Eq. (A2) in (A1) and using Eq. (2.4), we find that $\tilde{\mathbf{v}}_{\alpha\beta}(\mathbf{k}) \propto \delta_{\alpha\beta}$ is indeed appropriate provided that

$$\gamma_k = \frac{\hbar v^2}{E_k}\frac{\tau}{\tau_0}. \tag{A3}$$

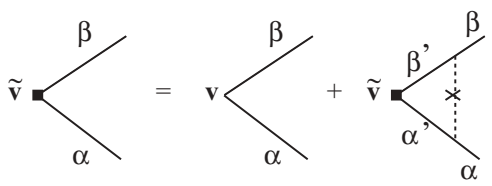

FIG. 10. Impurity vertex corrections for the velocity operator.

Here,

$$\frac{\hbar}{\tau} = 2\pi\nu u_0 \int \frac{d\Omega_{\mathbf{k}'}}{4\pi} \sum_{\alpha'} |\langle\alpha\mathbf{k}_F|\alpha'\mathbf{k}'_F\rangle|^2(1-\hat{\mathbf{k}}_F\cdot\hat{\mathbf{k}}'_F) \tag{A4}$$

is the transport scattering time. Therefore, the final result for the renormalized velocity is $\tilde{\mathbf{v}}_{\alpha\beta}(\mathbf{k}) = \mathbf{v}_{\alpha\beta}(\mathbf{k})(\tau/\tau_0)$.

APPENDIX B: EVALUATION OF $\delta\sigma_2$ IN SOME SIMPLE CASES

The expression for $\delta\sigma_2$ [depicted in Fig. 2(c)] reads as

$$\delta\sigma_2 \simeq -2\frac{e^2\hbar}{2\pi}\int_{\mathbf{k},\mathbf{k}'} \tilde{v}^x(\mathbf{k})\tilde{v}^x(\mathbf{k}')G^A(\mathbf{k}) \times G^A(\mathbf{k}')G^A(-\mathbf{k})G^A(-\mathbf{k}')G^R(-\mathbf{k}')G^R(\mathbf{k}) \times \sum_{\alpha\beta\alpha'\beta'} \Gamma^{\alpha\alpha'}_{\beta'\beta}(\mathbf{k},-\mathbf{k}',0)\frac{1}{W}\int\frac{d^2Q}{(2\pi)^2}C^{\beta\alpha}_{\alpha'\beta'}(\mathbf{k},\mathbf{k}',\mathbf{Q}), \tag{B1}$$

where the overall factor of 2 stems from the fact that the two diagrams in Fig. 2(c) give identical contribution, and the band indices α,β, etc., are summed over 1,2. For generic $(\epsilon_F - M)/M$, the calculation of $\delta\sigma_2$ is cumbersome. Here, we focus on two simple limits that are of interest: $(\epsilon_F - M)/M \ll 1$ and $(\epsilon_F - M)/M \gg 1$.

When $(\epsilon_F - M)/M \ll 1$, the momentum dependence of $|\alpha\mathbf{k}_F\rangle$ is negligible. Consequently, $C^{\beta\alpha}_{\alpha'\beta'}(\mathbf{k}_F,\mathbf{k}'_F,\mathbf{Q})$ and $\Gamma^{\alpha\alpha'}_{\beta'\beta}(\mathbf{k}_F,-\mathbf{k}'_F,0)$ become independent of $\mathbf{k}_F$ and $\mathbf{k}'_F$. Since the matrix elements of the velocity operator are odd under $\mathbf{k}\to-\mathbf{k}$ and $\mathbf{k}'\to-\mathbf{k}'$, it is clear that

$$\delta\sigma_2 \simeq 0. \tag{B2}$$

The limit of $(\epsilon_F - M)/M \gg 1$ is less trivial. In this regime, the Hamiltonian is approximately block diagonal both in absence and in presence of disorder because the disorder potential we take is spin and orbital independent. Therefore, we may focus on a 2×2 Hamiltonian describing a Weyl node with positive chirality:

$$h'(\mathbf{k}) = \hbar v\mathbf{k}\cdot\boldsymbol{\sigma} + V_0(\mathbf{r})\mathbf{1}_{2\times 2}, \tag{B3}$$

where $\mathbf{k} = k(\sin\theta\cos\phi, \sin\theta\sin\phi, \cos\theta)$. The result for $\delta\sigma$ obtained from such Hamiltonian needs to be multiplied by two at the end, as each block makes an equal contribution. The eigenstates for $h'(\mathbf{k})$ are $|+,\mathbf{k}\rangle = [\cos(\theta/2), \exp(i\phi)\sin(\theta/2)]^T$ and $|-,\mathbf{k}\rangle = [\sin(\theta/2), -\exp(i\phi)\cos(\theta/2)]^T$.

One significant simplification from Eq. (B3) is that there is only one band at the Fermi energy. This allows us to rewrite Eq. (B1) as

$$\delta\sigma_2 = -4\frac{e^2\hbar^3}{2\pi}u_0\frac{\tau^2}{\tau_0^2}\left[\int\frac{dk k^2}{(2\pi)^2}\frac{kv^2}{E_k}(G^A)^2G^R\right]^2\frac{1}{W}\int\frac{d^2Q}{(2\pi)^2} \times \int\frac{d\Omega_{\mathbf{k}}}{4\pi}\int\frac{d\Omega_{\mathbf{k}'}}{4\pi}\sin\theta\cos\phi\sin\theta'\cos\phi'\langle+,\mathbf{k}_F|+,\mathbf{k}'_F\rangle \times\langle+,-\mathbf{k}_F|+,-\mathbf{k}'_F\rangle C^{++}_{++}(\mathbf{k}_F,\mathbf{k}'_F,\mathbf{Q}), \tag{B4}$$

where the aforementioned extra factor of 2 has been accounted for. It is illustrative to compare Eq. (B4) with its counterpart in $\delta\sigma_1$:

$$\delta\sigma_1 = -2\frac{e^2\hbar^3}{2\pi}\frac{\tau^2}{\tau_0^2}\int\frac{dkk^2}{(2\pi)^2}\frac{k^2v^4}{E_k^2}(G^R)^2(G^A)^2 \times\frac{1}{W}\int\frac{d^2Q}{(2\pi)^2}\sin^2\theta\cos^2\phi\, C^{++}_{++}(\mathbf{k}_F,\mathbf{k}_F,\mathbf{Q}). \quad \text{(B5)}$$

In Sec. II, we detailed the steps to follow for the evaluation of Eq. (B5). By applying those same steps to Eq. (B4) and using

$$\int\frac{dkk^2}{2\pi^2}\frac{k^2}{E_k^2}(G^R)^2(G^A)^2 \simeq \frac{4\pi\nu\tau_0^3}{\hbar^5v^2} \quad \text{and} \quad \left[\int\frac{dkk^2}{(2\pi)^2}\frac{k}{E_k}(G^A)^2G^R\right]^2 u_0 \simeq -\frac{4\pi\nu\tau_0^3}{\hbar^5v^2}, \quad \text{(B6)}$$

we arrive at

$$\delta\sigma_2 = -\frac{1}{3}\delta\sigma_1 = -\frac{1}{3}G_q\ln\left(\frac{\tau_\phi}{\tau}\right). \quad \text{(B7)}$$

APPENDIX C: EVALUATION OF MATRIX ELEMENTS FOR $\hat{U}$

In this Appendix, we calculate the coefficients entering in Eq. (2.25). These coefficients generally depend on the frequency Ω and wave vector $\mathbf{Q}$ of the external perturbation. Even though only $\Omega = 0$ is needed for our evaluation of $\delta\sigma$, for completeness here we allow for $\Omega \neq 0$ as well.

The calculation is facilitated by rewriting Eq. (2.1) as

$$h(\mathbf{k}) = \sum_\mu \eta_\mu(\mathbf{k})\Lambda^\mu, \quad \text{(C1)}$$

where $\mu \in \{1,2,3,4\}$, $\eta_i(\mathbf{k}) = \hbar v k_i$, and $\Lambda^i = \sigma^i\tau^x$ for $i \in \{1,2,3\}$, $\eta_4(\mathbf{k}) = M$, and $\Lambda^4 = \mathbf{1}_2\,\tau^z$. Then, the finite-frequency retarded and advanced Green's functions read as

$$G^{R(A)}_{mn}(\mathbf{k},\Omega) = \frac{\epsilon^{R(A)}\delta^0_{mn} + \sum_\mu \eta_\mu\Lambda^\mu_{mn}}{[\epsilon^{R(A)}]^2 - E_k^2}, \quad \text{(C2)}$$

where $\epsilon^R \equiv \epsilon_F + i\gamma$ and $\epsilon^A \equiv \epsilon_F + \hbar\Omega - i\gamma$, with $\gamma \equiv \hbar/(2\tau_0)$ [cf. Eq. (2.5)]. Substituting Eq. (C2) in (2.19), we get

$$U^{ml}_{m'l'} = a\,\delta_{ml}\delta_{m'l'} + \sum_\mu b_\mu\,\Lambda^\mu_{m'l'}\delta_{ml} + \sum_\mu c_\mu\,\Lambda^\mu_{ml}\delta_{m'l'} + \sum_{\mu\nu} d_{\mu\nu}\,\Lambda^\mu_{ml}\Lambda^\nu_{m'l'}, \quad \text{(C3)}$$

where

$$a = u_0\int\frac{d^3k}{(2\pi)^3}\frac{\epsilon^R(\epsilon^A+\hbar\Omega)}{\left[(\epsilon^R)^2 - E^2_{-\mathbf{k}}\right]\left[(\epsilon^A+\hbar\Omega)^2 - E^2_{\mathbf{k}+\mathbf{Q}}\right]},$$

$$b_\mu = u_0\int\frac{d^3k}{(2\pi)^3}\frac{\epsilon^R d_\mu(\mathbf{k}+\mathbf{Q})}{\left[(\epsilon^R)^2 - E^2_{-\mathbf{k}}\right]\left[(\epsilon^A+\hbar\Omega)^2 - E^2_{\mathbf{k}+\mathbf{Q}}\right]},$$

$$c_\mu = u_0\int\frac{d^3k}{(2\pi)^3}\frac{(\epsilon^A+\hbar\Omega)d_\mu(-\mathbf{k})}{\left[(\epsilon^R)^2 - E^2_{-\mathbf{k}}\right]\left[(\epsilon^A+\hbar\Omega)^2 - E^2_{\mathbf{k}+\mathbf{Q}}\right]},$$

$$d_{\mu\nu} = u_0\int\frac{d^3k}{(2\pi)^3}\frac{d_\mu(-\mathbf{k})d_\nu(\mathbf{k}+\mathbf{Q})}{\left[(\epsilon^R)^2 - E^2_{-\mathbf{k}}\right]\left[(\epsilon^A+\hbar\Omega)^2 - E^2_{\mathbf{k}+\mathbf{Q}}\right]}, \quad \text{(C4)}$$

and $\mu,\nu \in \{1,2,3,4\}$. In the diffusive transport regime, namely $(\epsilon_F - M) \gg \gamma \gg (\hbar v Q, \hbar\Omega)$, the integrals in Eq. (C4) can be analytically performed and the outcome is

$$a \simeq a^{(0)}\left[1 - \frac{1}{12}\left(1 - \frac{M^2}{\epsilon_F^2}\right)\frac{\hbar^2v^2Q^2}{\gamma^2} - \frac{i\hbar\Omega}{2\gamma}\right],$$

$$b_1 = -c_1 \simeq \frac{i}{6}a^{(0)}\left(1 - \frac{M^2}{\epsilon_F^2}\right)\frac{\hbar vQ_x}{\gamma}, \quad b_2 = -c_2 \simeq \frac{i}{6}a^{(0)}\left(1 - \frac{M^2}{\epsilon_F^2}\right)\frac{\hbar vQ_y}{\gamma}, \quad b_4 = c_4 = \frac{M}{\epsilon_F}a,$$

$$d_{11} \simeq -\frac{1}{3}\left(1 - \frac{M^2}{\epsilon_F^2}\right)a^{(0)}\left[1 - \frac{1}{20}\left(1 - \frac{M^2}{\epsilon_F^2}\right)\frac{(3Q_x^2+Q_y^2)\hbar^2v^2}{\gamma^2} - \frac{i\hbar\Omega}{2\gamma}\right],$$

$$d_{22} \simeq -\frac{1}{3}\left(1 - \frac{M^2}{\epsilon_F^2}\right)a^{(0)}\left[1 - \frac{1}{20}\left(1 - \frac{M^2}{\epsilon_F^2}\right)\frac{(3Q_y^2+Q_x^2)\hbar^2v^2}{\gamma^2} - \frac{i\hbar\Omega}{2\gamma}\right],$$

$$d_{33} \simeq -\frac{1}{3}\left(1 - \frac{M^2}{\epsilon_F^2}\right)a^{(0)}\left[1 - \frac{1}{20}\left(1 - \frac{M^2}{\epsilon_F^2}\right)\frac{\hbar^2v^2Q^2}{\gamma^2} - \frac{i\hbar\Omega}{2\gamma}\right],$$

$$d_{44} \simeq \frac{M^2}{\epsilon_F^2}a, \quad d_{12} = d_{21} \simeq a^{(0)}\frac{1}{30}\left(1 - \frac{M^2}{\epsilon_F^2}\right)^2\frac{\hbar^2v^2Q_xQ_y}{\gamma^2},$$

$$d_{14} = -d_{41} \simeq -ia^{(0)}\frac{M}{\epsilon_F}\left(1 - \frac{M^2}{\epsilon_F^2}\right)\frac{\hbar vQ_x}{\gamma}, \quad d_{24} = -d_{42} \simeq -ia^{(0)}\frac{M}{\epsilon_F}\left(1 - \frac{M^2}{\epsilon_F^2}\right)\frac{\hbar vQ_y}{\gamma}, \quad \text{(C5)}$$

where $a^{(0)} \equiv [2(1 + M^2/\epsilon_F^2)]^{-1}$, and the elements omitted above are zero. It is worth noting that Eq. (C5) can be used to investigate the dynamical spin-charge coupling in doped TIs. Since this task is not directly related to the theme of this paper, it will be pursued elsewhere.

APPENDIX D: CLASSICAL CONDUCTIVITY OF TWO COUPLED LAYERS

In this Appendix, we analyze the classical conductivity of two coupled layers. The current in layer i is given by $\mathbf{j}_i = \sum_j \sigma_{ij}\mathbf{E}_j$. It is illustrative to write σ_{ij} in terms of the diffusive density-density response, using the continuity equation

$$\frac{\partial \rho_i}{\partial t} + \nabla \cdot \mathbf{j} + \lambda \sum_j (\rho_j - \rho_i) = 0 \tag{D1}$$

along with the constitutive equation $\mathbf{j}_i = -D_i \nabla \rho_i - e^2 \nu_i D_i \mathbf{E}_i$. λ is the interlayer tunneling rate. Thus, it follows that

$$\sigma_{ij}(\mathbf{q},\omega) = -\frac{i\omega}{q^2}\chi_{ij} + \frac{\lambda}{q^2}\sum_k (\chi_{ij} - \chi_{kj}), \tag{D2}$$

where $\chi_{ij}(\mathbf{q},\omega) = e^2 \nu_j D_j q^2 p_{ij}(\mathbf{q},\omega)$ is the density-density response function and

$$p_{ij}(\mathbf{q},\omega) = \begin{cases} \tilde{p}_i^{(0)} \big/ \big(1 - \lambda^2 p_1^{(0)} p_2^{(0)}\big) & \text{if } i = j, \\ \lambda \tilde{p}_1^{(0)} \tilde{p}_2^{(0)} \big/ \big(1 - \lambda^2 p_1^{(0)} p_2^{(0)}\big) & \text{if } i \neq j \end{cases} \tag{D3}$$

with $\tilde{p}_i^{(0)} \equiv (D_i q^2 - i\omega + \lambda)^{-1}$. The dressed diffusion probability p_{ii}, derived here from the continuity equation, has the identical form as Eq. (3.6), which was derived microscopically in Sec. III B. Here, ω and $\mathbf{q}$ are the frequency and momentum associated with the applied electric field. A straightforward calculation shows that $\sigma_{12} = \sigma_{21} = 0$ when $\mathbf{E}_i$ is spatially uniform ($\mathbf{q} = 0$).

APPENDIX E: EQUATIONS FOR COUPLED COOPERONS

In the first part of this Appendix, we present an alternative derivation for the results of Sec. III B. In the second part of the Appendix, we generalize the derivation to make it suitable for TI thin films with $\tau_{\phi 1} \ll \tau_v$, which contain two gapless singlet cooperons in the bulk and one gapless singlet cooperon on the surface. The outcome of such generalization is the third line of Eq. (3.17).

1. Two 2D layers without spin-orbit coupling

In this section, we use "1" and "2" to label the two layers. The relevant cooperon modes are then C_{11}, C_{12}, C_{21}, and C_{22}. Recognizing that cooperons must obey a diffusion equation in absence of phase relaxation, we posit the following coupled equations:

$$\begin{aligned}
\big(D_1 Q^2 + \tau_{\phi 1}^{-1}\big)C_{11} + \lambda(C_{11} - C_{21}) &= \hbar/\big(2\pi \nu_1 \tau_{d1}^2\big), \\
\big(D_2 Q^2 + \tau_{\phi 2}^{-1}\big)C_{21} + \lambda(C_{21} - C_{11}) &= 0, \\
\big(D_2 Q^2 + \tau_{\phi 2}^{-1}\big)C_{22} + \lambda(C_{22} - C_{12}) &= \hbar/\big(2\pi \nu_2 \tau_{d2}^2\big), \\
\big(D_1 Q^2 + \tau_{\phi 1}^{-1}\big)C_{12} + \lambda(C_{12} - C_{22}) &= 0,
\end{aligned} \tag{E1}$$

where λ is the interlayer tunneling rate. Note that the source term appears only for the diagonal terms of the 2×2 cooperon matrix. The solution of Eq. (E1) reads as

$$\begin{aligned}
C_{11} &= \frac{\hbar}{2\pi \nu_1 \tau_1^2} \frac{D_2 Q^2 + \tilde{\tau}_{\phi 2}^{-1}}{\big(D_1 Q^2 + \tilde{\tau}_{\phi 1}^{-1}\big)\big(D_2 Q^2 + \tilde{\tau}_{\phi 2}^{-1}\big) - \lambda^2}, \\
C_{22} &= \frac{\hbar}{2\pi \nu_2 \tau_2^2} \frac{D_1 Q^2 + \tilde{\tau}_{\phi 1}^{-1}}{\big(D_1 Q^2 + \tilde{\tau}_{\phi 1}^{-1}\big)\big(D_2 Q^2 + \tilde{\tau}_{\phi 2}^{-1}\big) - \lambda^2}, \\
C_{12} &= C_{21} = \frac{\lambda}{D_2 Q^2 + \tilde{\tau}_{\phi 2}^{-1}} C_{11},
\end{aligned} \tag{E2}$$

where $\tilde{\tau}_{\phi i}^{-1} \equiv \tau_{\phi i}^{-1} + \lambda$. The expressions for C_{11} and C_{22} agree with Eq. (3.6). In addition, C_{12} and C_{21} agree with the expressions for p_{12} and p_{21} derived in Appendix D (where we discussed the classical diffusive conductivity). C_{ii} of Eq. (E1) is equivalent to C_{ii}^{ii} of Fig. 3. Likewise, C_{12} and C_{21} of Eq. (E1) correspond to C_{22}^{11} and C_{11}^{22} of Fig. 3. Although C_{12} and C_{21} are nonzero, they do not contribute to $\delta\sigma$ because the velocity operator is diagonal in the layer index. Therefore, we reproduce the expression of Sec. III B for $\delta\sigma$.

2. TI film with two gapless bulk cooperons and one gapless surface cooperon

In this section, we use "1" and "3" to label the two bulk cooperons, and "2" to label the surface cooperon. The generalization of Eq. (E1) is

$$\begin{aligned}
\big(D_1 Q^2 + \tau_{\phi 1}^{-1}\big)C_{11} + \lambda(C_{11} - C_{21}) &= \hbar/\big(2\pi \nu_1 \tau_{d1}^2\big), \\
\big(D_2 Q^2 + \tau_{\phi 2}^{-1}\big)C_{21} + \lambda(2C_{21} - C_{11} - C_{31}) &= 0, \\
\big(D_1 Q^2 + \tau_{\phi 1}^{-1}\big)C_{31} + \lambda(C_{31} - C_{21}) &= 0,
\end{aligned} \tag{E3}$$

$$\begin{aligned}
\big(D_1 Q^2 + \tau_{\phi 1}^{-1}\big)C_{12} + \lambda(C_{12} - C_{22}) &= 0, \\
\big(D_2 Q^2 + \tau_{\phi 2}^{-1}\big)C_{22} + \lambda(2C_{22} - C_{12} - C_{32}) &= \hbar/\big(2\pi \nu_2 \tau_{d2}^2\big), \\
\big(D_1 Q^2 + \tau_{\phi 1}^{-1}\big)C_{32} + \lambda(C_{32} - C_{22}) &= 0,
\end{aligned} \tag{E4}$$

and

$$\begin{aligned}
\big(D_1 Q^2 + \tau_{\phi 1}^{-1}\big)C_{13} + \lambda(C_{13} - C_{23}) &= 0, \\
\big(D_2 Q^2 + \tau_{\phi 2}^{-1}\big)C_{23} + \lambda(2C_{23} - C_{13} - C_{33}) &= 0, \\
\big(D_1 Q^2 + \tau_{\phi 1}^{-1}\big)C_{33} + \lambda(C_{33} - C_{23}) &= \hbar/\big(2\pi \nu_1 \tau_{d1}^2\big).
\end{aligned} \tag{E5}$$

Once again, in Eqs. (E3)–(E5) the source term appears for the diagonal components of the 3×3 cooperon matrix. In addition, a factor of 2 has been multiplied in front of some tunneling rates associated to surface cooperons. The rationale behind this is that the cooperon on the surface can decay into two bulk modes, i.e., the effective decay rate becomes $\tau_{\phi 2}^{-1} + 2\lambda$. Aside from this, we have assumed a unique tunneling rate λ between all pairs of cooperons.

The quantum correction to conductance can be written as

$$\delta G = 2\frac{e^2}{\hbar^2}\nu_1 D_1 \tau_{d1}^2 \int_{\mathbf{Q}} (C_{11} + C_{33}) + 2\frac{e^2}{\hbar^2}\nu_2 D_2 \tau_{d2}^2 \int_{\mathbf{Q}} C_{22}. \tag{E6}$$

Solving Eqs. (E3)–(E5) requires some algebra. The results for the cooperons of interest are

$$C_{11} = C_{33} = \frac{\hbar}{2\pi\nu_1\tau_{d1}^2}\frac{\left(D_1Q^2+\tilde{\tau}_{\phi1}^{-1}\right)\left(D_2Q^2+\tilde{\tau}_{\phi2}^{-1}+\lambda\right)-\lambda^2}{\left(D_1Q^2+\tilde{\tau}_{\phi1}^{-1}\right)\left[\left(D_1Q^2+\tilde{\tau}_{\phi1}^{-1}\right)\left(D_2Q^2+\tilde{\tau}_{\phi2}^{-1}+\lambda\right)-2\lambda^2\right]},$$
$$C_{22} = \frac{\hbar}{2\pi\nu_2\tau_{d2}^2}\frac{D_1Q^2+\tilde{\tau}_{\phi1}^{-1}}{\left(D_1Q^2+\tilde{\tau}_{\phi1}^{-1}\right)\left(D_2Q^2+\tilde{\tau}_{\phi2}^{-1}+\lambda\right)-2\lambda^2}, \tag{E7}$$

which are not illuminating expressions. It is better to rewrite them as

$$C_{11} = C_{33} = \frac{\hbar}{2\pi\nu_1\tau_{d1}^2}\frac{1}{D_1}\left[\frac{X}{Q^2+q_x^2}+\frac{Y}{Q^2+q_y^2}+\frac{Z}{Q^2+q_z^2}\right],$$
$$C_{22} = \frac{\hbar}{2\pi\nu_2\tau_{d2}^2}\frac{1}{D_2}\left[\frac{A}{Q^2+q_a^2}+\frac{B}{Q^2+q_b}\right], \tag{E8}$$

so that Eq. (E6) transforms into

$$\delta G = \frac{e^2}{\pi\hbar}\int_{\mathbf{Q}}\left[2\frac{X}{Q^2+q_x^2}+2\frac{Y}{Q^2+q_y^2}+2\frac{Z}{Q^2+q_z^2}+\frac{A}{Q^2+q_a^2}+\frac{B}{Q^2+q_b^2}\right]. \tag{E9}$$

Comparing Eqs. (E7) and (E8), we arrive at

$$A = \frac{\frac{1}{D_1\tilde{\tau}_{\phi1}}-q_a^2}{q_b^2-q_a^2},\quad B = 1-A,\quad X = \frac{\left(D_1q_x^2-\tilde{\tau}_{\phi1}^{-1}\right)\left(D_2q_x^2-\tilde{\tau}_{\phi2}^{-1}-\lambda\right)-\lambda^2}{D_1D_2\left(q_x^2-q_y^2\right)\left(q_x^2-q_z^2\right)},$$
$$Y = \frac{D_2q_y^2\tilde{\tau}_{\phi1}^{-1}-\tilde{\tau}_{\phi1}^{-1}\left(\tilde{\tau}_{\phi2}^{-1}+\lambda\right)+D_1q_y^2\left(-D_2q_y^2+\tilde{\tau}_{\phi2}^{-1}+\lambda\right)+\lambda^2}{D_1D_2\left(q_x^2-q_y^2\right)\left(q_y^2-q_z^2\right)},$$
$$Z = \frac{D_2q_z^2\tilde{\tau}_{\phi1}^{-1}-\tilde{\tau}_{\phi1}^{-1}\left(\tilde{\tau}_{\phi2}^{-1}+\lambda\right)+D_1q_z^2\left(-D_2q_z^2+\tilde{\tau}_{\phi2}^{-1}+\lambda\right)+\lambda^2}{D_1D_2\left(q_x^2-q_z^2\right)\left(q_z^2-q_y^2\right)}, \tag{E10}$$

and

$$2q_{a(b)}^2 = \frac{1}{D_1\tilde{\tau}_{\phi1}}+\frac{1}{D_2\tilde{\tau}_{\phi2}}+\frac{\lambda}{D_2}\pm\sqrt{\left(\frac{1}{D_1\tilde{\tau}_{\phi1}}-\frac{1}{D_2\tilde{\tau}_{\phi2}}-\frac{\lambda}{D_2}\right)^2+\frac{8\lambda^2}{D_1D_2}},\quad q_{x(y)}^2 = q_{a(b)}^2,\quad q_z^2 = 1/(D_1\tilde{\tau}_{\phi1}). \tag{E11}$$

Note that $q_{a(b)} = q_{x(y)}$, which will be important below. Also note that the expressions for A, B, and $q_{a(b)}$ are identical to the ones in Sec. III B, except for the following difference: the effective inelastic scattering rate for layer 2 is now $\tau_{\phi2}^{-1}+2\lambda$ instead of $\tau_{\phi2}^{-1}+\lambda$, for the reason explained above.

Although Eqs. (E10) and (E11) look cumbersome, after substituting Eq. (E11) back in (E10), we find some remarkable simplifications. In particular,

$$Z = 1/2\ ,\quad 2X+A = 1,\quad \text{and}\quad 2Y+B = 1. \tag{E12}$$

Replacing these in Eq. (E9) immediately leads to

$$\delta G = \frac{e^2}{\pi\hbar}\int_{\mathbf{Q}}\left[\frac{1}{Q^2+q_a^2}+\frac{1}{Q^2+q_b^2}+\frac{1}{Q^2+q_z^2}\right]. \tag{E13}$$

In consequence, we recover the third line of Eq. (3.17) for the low-field magnetoconductance:

$$\frac{\Delta G}{G_q} = \frac{1}{2}\left[f\left(\frac{H_a}{H}\right)+f\left(\frac{H_b}{H}\right)+f\left(\frac{H_z}{H}\right)\right], \tag{E14}$$

where $H_a = \hbar q_a^2/(4e)$, etc. As a reality check, let us take some simple limits. First, consider the case of no bulk-surface coupling $\lambda\to 0$. In this case, $H_a = H_z = \hbar/(4eD_1\tau_{\phi1})$ and $H_b = \hbar/(4eD_2\tau_{\phi2})$, which produces

$$\frac{\Delta G}{G_q} = \frac{1}{2}\left[2f\left(\frac{H_a}{H}\right)+f\left(\frac{H_b}{H}\right)\right]. \tag{E15}$$

This is indeed the result one would have expected when bulk and surface are decoupled.

Second, suppose both $\tau_{\phi1}$ and $\tau_{\phi2}$ are infinitely large, for arbitrary tunneling rate. Then, it follows that $H_b = 0$,

$$H_a = \frac{\hbar}{4e}\lambda\left(\frac{1}{D_1}+\frac{2}{D_2}\right),\quad \text{and}\quad H_z = \frac{\hbar}{4e}\frac{\lambda}{D_1}. \tag{E16}$$

Then,

$$\frac{\Delta G}{G_q} = \frac{1}{2}\left[f\left(\frac{H_a}{H}\right)+f\left(\frac{H_z}{H}\right)\right]. \tag{E17}$$

The fact that $H_b = 0$ means that we recover the conventional WAL case (as we should when the phase relaxation times are infinitely long).

Finally, consider the case of very strong tunneling between bulk and surface states. In this case, H_a and H_z become very large ($\propto\lambda$), whereas H_b becomes independent of λ.

Consequently,

$$\frac{\Delta G}{G_q} = \frac{1}{2} f\left(\frac{H_b}{H}\right), \tag{E18}$$

as if we had a single channel contributing to WAL. This seems to make sense too because when tunneling is strong, C_{ii} are strongly coupled to one another ($i = 1,2,3$).

APPENDIX F: SOME SPECIAL CASES OF EQ. (3.17)

In this Appendix, we analyze some simple limiting cases of Eq. (3.17), which considers a single TI surface coupled to bulk states. First, suppose that surface-bulk tunneling is strong, so that $\tau_{ti} \ll \tau_{\phi i}$ for $i = 1,2$. In this case, $(H_a, H_c, \tilde{H}_1) \gg (H_b, H_d)$ and thus Eq. (3.17) turns into

$$\frac{\Delta G}{G_q} = \frac{1}{2}\begin{cases} f(H_b/H) & \text{if } \tilde{\tau}_H \ll \tau_s, \\ f(H_b/H) & \text{if } \tilde{\tau}_H \gg (\tau_v, \tau_s), \\ f(H_d/H) & \text{if } \tilde{\tau}_H \ll \tau_v, \end{cases} \tag{F1}$$

where $H_b \simeq \hbar/(4e)(1/\tau_{\phi 1} + 1/\tau_{\phi 2})/(D_1 + D_2)$ and $H_d \simeq \hbar/(4e)(2/\tau_{\phi 1} + 1/\tau_{\phi 2})/(2D_1 + D_2)$. For simplicity, we have taken $\tau_{t1} = \tau_{t2}$, but this assumption can be easily relaxed. In sum, WL is *not* possible when the bulk-surface coupling is strong, and the film exhibits conventional WAL ($\alpha = 1/2$) regardless of the bulk carrier concentration.

Next, we consider a weak surface-bulk tunneling, so that $\tau_{ti} \gg \tau_{\phi i}$ for $i = 1,2$. In this case, the outcome depends on whether $D_1\tau_{\phi 1} > D_2\tau_{\phi 2}$ or $D_1\tau_{\phi 1} < D_2\tau_{\phi 2}$. Without loss of generality, suppose that $D_1\tau_{\phi 1} > D_2\tau_{\phi 2}$. Then, Eq. (3.17) yields

$$\frac{\Delta G}{G_q} \simeq \frac{1}{2}\begin{cases} f(H_{\phi 2}/H) - 2f(H_{\phi 1}/H) & \text{if } \tilde{\tau}_H \ll \tau_s, \\ f(H_{\phi 2}/H) + f(H_{\phi 1}/H) & \text{if } \tilde{\tau}_H \gg (\tau_v, \tau_s), \\ f(H_{\phi 2}/H) + 2f(H_{\phi 1}/H) & \text{if } \tilde{\tau}_H \ll \tau_v, \end{cases} \tag{F2}$$

where $H_{\phi i} = \hbar/(4eD_i\tau_{\phi i})$ for $i = 1,2$. When $H_{\phi 1}$ and $H_{\phi 2}$ are of the same order, the first line of Eq. (F2) displays WL with $\alpha = -1/2$ and the third line exhibits WAL with $\alpha = 3/2$. If instead $H_{\phi 1} \ll H_{\phi 2}$, ΔG is the same as if there were no surface states. This latter regime can be experimentally accessible by, e.g., depositing magnetic impurities on the surface of the TI.

Last, we consider the case $\tau_{t1} \gg \tau_{\phi i} \gg \tau_{t2}$ for $i = 1,2$. This situation may be relevant for some thicker TI films where $\tau_{t1}/\tau_{t2} = W\nu_1/\nu_2 \gg 1$ (for thicker films, surface states have more bulk states to decay onto). The resulting magnetoconductance is once again as though there were no surface states:

$$\frac{\Delta G}{G_q} = \begin{cases} -f(H_{\phi 1}/H) & \text{if } \tilde{\tau}_H \ll \tau_s, \\ \frac{1}{2}f(H_{\phi 1}/H) & \text{if } \tilde{\tau}_H \gg (\tau_v, \tau_s), \\ f(H_{\phi 1}/H) & \text{if } \tilde{\tau}_H \ll \tau_v. \end{cases} \tag{F3}$$

[1] For reviews see, e.g., J. Moore, Nature (London) **464**, 194 (2010); M. Z. Hasan and C. L. Kane, Rev. Mod. Phys. **82**, 3045 (2010); X.-L. Qi and S.-C. Zhang, *ibid.* **83**, 1057 (2011).

[2] For a review see, e.g., M. Z. Hasan, D. Hsieh, Y. Xia, L. A. Wray, S.-Y. Xu, and C. L. Kane, arXiv:1105.0396.

[3] Z. Alpichshev, J. G. Analytis, J.-H. Chu, I. R. Fisher, Y. L. Chen, Z. X. Shen, A. Fang, and A. Kapitulnik, Phys. Rev. Lett. **104**, 016401 (2010); J. Seo, P. Roushan, H. Beidenkopf, Y. S. Hor, R. J. Cava, and A. Yazdani, Nature (London) **466**, 343 (2010).

[4] For a review see, e.g., D. Culcer, Phys. E (Amsterdam) **44**, 860 (2012).

[5] See, e.g., D. Kim, S. Cho, N. P. Butch, P. Syers, K. Kirshenbaum, S. Adam, J. Paglione, and M. S. Fuhrer, Nat. Phys. doi: 10.1038/nphysS2286 (2012); G. Zhang, H. Qin, J. Chen, X. He, L. Lu, Y. Li, and K. Wu, Adv. Funct. Mater. **21**, 2351 (2011).

[6] J. Chen, H. J. Qin, F. Yang, J. Liu, T. Guan, F. M. Qu, G. H. Zhang, J. R. Shi, X. C. Xie, C. L. Yang, K. H. Wu, Y. Q. Li, and L. Lu, Phys. Rev. Lett. **105**, 176602 (2010).

[7] J. G. Checkelsky, Y. S. Hor, R. J. Cava, and N. P. Ong, Phys. Rev. Lett. **106**, 196801 (2011).

[8] J. Wang, A. M. DaSilva, C.-Z. Chang, K. He, J. K. Jain, N. Samarth, X.-C. Ma, Q. K. Xue, and M. H. W. Chan, Phys. Rev. B **83**, 245438 (2011).

[9] H.-T. He, G. Wang, T. Zhang, I.-K. Sou, G. K. L. Wong, J.-N. Wang, H.-Z. Lu, S.-Q. Shen, and F.-C. Zhang, Phys. Rev. Lett. **106**, 166805 (2011).

[10] J. Chen, X. Y. He, K. H. Wu, Z. Q. Ji, L. Lu, J. R. Shi, J. H. Smet, and Y. Q. Li, Phys. Rev. B **83**, 241304 (2011).

[11] H. Steinberg, J. B. Laloe, V. Fatemi, J. S. Moodera, and P. Jarillo-Herrero, Phys. Rev. B **84**, 233101 (2011).

[12] S. S. Hong, J. J. Cha, D. Kong, and Y. Cui, Nat. Commun. doi: 10.1038/ncomms1771 (2012).

[13] For reviews see, e.g., E. Akkermans and G. Montambaux, *Mesoscopic Physics of Electrons and Photons* (Cambridge University Press, Cambridge, 2007); B. L. Altshuler, A. G. Aronov, D. E. Khmelnitskii, and A. I. Larkin, *Quantum Theory of Solids* (MIR Publishers, Moscow, 1982).

[14] Recently, we have been informed of a new experiment that reports on the first observation of WL (negative magnetoresistance) in TI thin films; see L. Zhang, R. Hammond, M. Dolev, M. Liu, A. Palevski, and A. Kapitulnik, arXiv:1205.5832.

[15] S. Hikami, A. I. Larkin, and Y. Nagaoka, Prog. Theor. Phys. **63**, 707 (1980).

[16] H.-Z. Lu, J. Shi, and S.-Q. Shen, Phys. Rev. Lett. **107**, 076801 (2011).

[17] G. Tkachov and E. M. Hankiewicz, Phys. Rev. B **84**, 035444 (2011).

[18] H.-Z. Lu and S.-Q. Shen, Phys. Rev. B **84**, 125138 (2011).

[19] S. Murakami, New J. Phys. **9**, 356 (2007); A. A. Burkov and L. Balents, Phys. Rev. Lett. **107**, 127205 (2011); X. Wan, A. M. Turner, A. Vishwanath, and S. Y. Savrasov, Phys. Rev. B **83**, 205101 (2011); P. Hosur, S. A. Parameswaran, and A. Vishwanath, Phys. Rev. Lett. **108**, 046602 (2012).

[20] E. McCann, K. Kechedzhi, V. I. Falko, H. Suzuura, T. Ando, and B. L. Altshuler, Phys. Rev. Lett. **97**, 146805 (2006).

[21] H. Zhang, C.-X. Liu, X.-L. Qi, X. Dai, Z. Fang, and S.-C. Zhang, Nat. Phys. **5**, 438 (2009); H.-J. Zhang, C.-X. Liu, X.-L. Qi, X.-Y.

Deng, X. Dai, S.-C. Zhang, and Z. Fang, Phys. Rev. B **80**, 085307 (2009).

[22]I. Garate, J. Sinova, T. Jungwirth, and A. H. MacDonald, Phys. Rev. B **79**, 155207 (2009).

[23]S.-Y. Xu, Y. Xia, L. A. Wray, S. Jia, F. Meier, J. H. Dil, J. Osterwalder, B. Slomski, A. Bansil, H. Lin, R. J. Cava, and M. Z. Hasan, Science **332**, 560 (2011).

[24]H. Fukuyama, Suppl. Prog. Theor. Phys. **69**, 220 (1980); J. Phys. Soc. Jpn. **49**, 649 (1980).

[25]G. Bergmann, Phys. Rev. B **39**, 11280 (1989).

[26]See, e.g., S. M. Sze, *Semiconductor Devices*, 2nd ed. (Wiley, New York, 2002).

[27]D. T. Son and B. Z. Spivak, arXiv:1206.1627.